

NASA CR-818

APERTURE REFLECTION COEFFICIENT OF A  
PARALLEL-PLATE WAVEGUIDE BY  
WEDGE DIFFRACTION ANALYSIS

By R. C. Rudduck and L. L. Tsai

Distribution of this report is provided in the interest of information exchange. Responsibility for the contents resides in the author or organization that prepared it.

Issued by Originator as Technical Report 1691-20

Prepared under Grant No. NsG-448 by  
THE OHIO STATE UNIVERSITY  
ELECTRO SCIENCE LABORATORY  
(formerly Antenna Laboratory)  
Columbus, Ohio

for

NATIONAL AERONAUTICS AND SPACE ADMINISTRATION

---

For sale by the Clearinghouse for Federal Scientific and Technical Information  
Springfield, Virginia 22151 - CFSTI price \$3.00

## ABSTRACT

Wedge diffraction theory is applied to analyze the aperture reflection coefficients of TEM and  $TE_{01}$  parallel-plate waveguide apertures. Fields of the guides are used in conjunction with the guide effective apertures to obtain the reflection coefficients and hence aperture admittances. Calculated results of reflection coefficients versus guide widths are verified by measurements and results from other methods of analysis.

## TABLE OF CONTENTS

	Page
I. INTRODUCTION	1
II. FIELDS OF PARALLEL-PLATE WAVEGUIDES	1
A. <u>TEM Mode</u>	1
B. <u>TE<sub>01</sub> Mode</u>	6
III. EFFECTIVE APERTURE	11
A. <u>TEM Mode</u>	11
B. <u>TE<sub>01</sub> Mode</u>	13
IV. REFLECTION COEFFICIENT OF APERTURE	15
A. <u>TEM Mode</u>	15
B. <u>TE<sub>01</sub> Mode</u>	17
V. NUMERICAL RESULTS	20
A. <u>TEM Mode</u>	20
B. <u>TE<sub>01</sub> Mode</u>	22
VI. CONCLUSIONS	22
APPENDIX	39
REFERENCES	40

# APERTURE REFLECTION COEFFICIENT OF A PARALLEL-PLATE WAVEGUIDE BY WEDGE DIFFRACTION ANALYSIS

## I. INTRODUCTION

The aperture admittance or the reflection coefficient of parallel-plate guide apertures is analyzed by application of wedge diffraction. This technique has been successfully applied to the calculation of the radiation patterns of parallel-plate guides<sup>1</sup> and coupling between such guides.<sup>2</sup>

The diffracted fields from the aperture of the parallel-plate guide are analyzed in terms of the diffractions of plane and cylindrical waves incident upon a perfectly conducting wedge.<sup>3</sup> The appropriate equations for the far fields of the aperture are given in Section II. The effective aperture of the guide is derived in Section III. The reflection coefficient of the guide aperture is derived from the effective aperture in Section IV. Numerical results are presented in Section V along with comparisons with measured reflection coefficients and those calculated by other methods.

## II. FIELDS OF PARALLEL-PLATE WAVEGUIDES

### A. TEM Mode

By the edge-diffraction method the field diffracted from the parallel-plate guide aperture is obtained by superimposing the diffracted fields from each edge. The field from each edge is that caused by the incident wave illumination and subsequent interactions of the diffracted waves from each edge. In this discussion, fields in the far field region are the only ones of interest. Consequently, a field quantity may be represented by

$$(1) \quad F = \frac{e^{-j\left(kr + \frac{\pi}{4}\right)}}{\sqrt{2\pi kr}} \quad R = \frac{e^{-jkr}}{\sqrt{r}} \quad D ,$$

where D is commonly denoted as a diffraction coefficient and R is denoted here as a ray.

For the TEM mode the component of the field perpendicular to the plane of Fig. 1 is the magnetic field and the fields radiated from the guide are everywhere transverse magnetic (TM). The incident modal field in

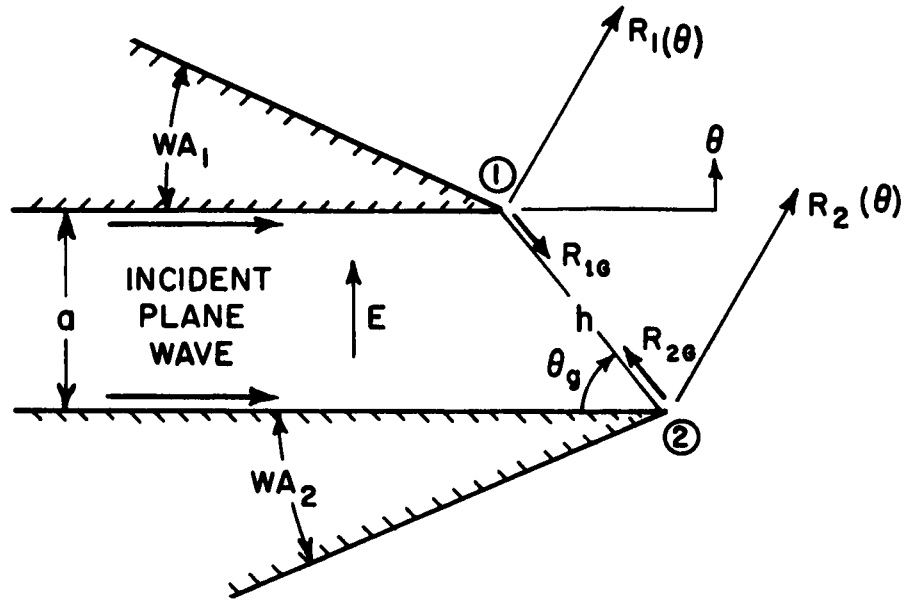


Fig. 1. TEM mode in a parallel-plate waveguide.

the guide is uniform across the guide cross section and thus the incident power flow for a unit-amplitude magnetic field is given by

$$(2) \quad P_0 = a Z_0, \quad Z_0 = \sqrt{\mu_0 / \epsilon_0} \quad .$$

The modal current associated with this mode is given by

$$(3) \quad I_0 = \sqrt{a} \quad .$$

The first-order diffracted rays which result from the incident wave are given by

$$(4) \quad R_1^{(1)}(\theta) = \frac{1}{n_1} \sin \frac{\pi}{n_1} \left( \frac{1}{\cos \frac{\pi}{n_1} - \cos \frac{\pi + \theta}{n_1}} \right)$$

and

$$(5) \quad R_2^{(1)}(\theta) = \frac{1}{n_2} \sin \frac{\pi}{n_2} e^{-jka \cot \theta_g} \left( \frac{1}{\cos \frac{\pi}{n_2} - \cos \frac{\pi - \theta}{n_2}} \right) ,$$

where the subscript denotes edge and the superscript denotes the order of diffraction.

The interactions between the wedges are treated in terms of multiple diffractions between the edges. Each diffracted wave appears to be a cylindrical wave emanating from a particular edge. Thus each subsequent diffraction may be approximated by the diffraction of a cylindrical wave by the opposite wedge. The first-order wave from edge 1 causes a second-order diffraction at edge 2 which, by assuming cylindrical wave illumination, is given by

$$(6) \quad R_2^{(2)}(\theta) = R_{1G}^{(1)} [V_B(h, \pi - \theta - \theta_g) + V_B(h, \pi - \theta + \theta_g)] \\ = R_{1G}^{(1)} V_{1G}(\theta) ,$$

where

$$(7) \quad R_{1G}^{(1)} = R_1^{(1)}(-\theta_g) .$$

There are subsequent diffractions which result in third- and higher-orders of diffraction from edge 2. However, the total illumination from edge 1 can be expressed as

$$(8) \quad R_{1G} = R_1(-\theta_g) ,$$

where  $R_1(\theta)$  is the total diffracted ray from edge 1. Consequently, the total higher-order diffraction (i.e., second-order and higher) from edge 2 is given by

$$(9) \quad R_2^{(h)}(\theta) = R_{1G} [V_B(h, \pi - \theta - \theta_g) + V_B(h, \pi - \theta + \theta_g)] \quad .$$

Thus the total diffracted wave from edge 2 is given by

$$(10) \quad R_2(\theta) = R_2^{(1)}(\theta) + R_2^{(h)}(\theta) \quad .$$

It should be noted that  $R_{1G}$  and, consequently,  $R_2^{(h)}$  and  $R_2$  are unknown at this point. Two singly diffracted rays,

$$(11) \quad R_{2G}^{(1)} = R_2^{(1)}(\pi - \theta_g) \quad .$$

and

$$(12) \quad R_{1P}^{(1)} = R_1^{(1)}\left(-\frac{\pi}{2}\right) \quad ,$$

produce the doubly diffracted wave from edge 1, as given by

$$(13) \quad \begin{aligned} R_1^{(2)}(\theta) &= R_{2G}^{(1)} [V_B(h, \theta + \theta_g) + V_B(h, 2\pi + \theta - \theta_g)] \\ &\quad + R_{1P}^{(1)} \left[ V_B\left(2a, \frac{\pi}{2} + \theta\right) + V_B\left(2a, \frac{3\pi}{2} + \theta\right) \right] \\ &= R_{2G}^{(1)} V_{2G}(\theta) + R_{1P}^{(1)} V_{1P}(\theta) \quad . \end{aligned}$$

The total higher-order illumination of edge 1 is given by

$$(14) \quad R_{2G} = R_2(\pi - \theta_g)$$

and

$$(15) \quad R_{1P} = R_1\left(-\frac{\pi}{2}\right) \quad .$$

Thus the total higher-order diffraction from edge 1 is given by

$$(16) \quad R_1^{(h)}(\theta) = R_{2G} V_{2G}(\theta) + R_{1P} V_{1P}(\theta) \quad .$$

Consequently, the total diffraction from edge 1 is given by

$$(17) \quad R_1(\theta) = R_1^{(1)}(\theta) + R_1^{(h)}(\theta) .$$

The diffracted waves from edges 1 and 2 are given in terms of the unknown illuminating rays  $R_{1G}$ ,  $R_{2G}$ , and  $R_{1P}$ . However, these three rays can be determined by the solution of three simultaneous linear equations formed by expressing each unknown ray in terms of Eq. (10) or Eq. (17):

$$(18) \quad \begin{aligned} R_{1G} &= R_{1G}^{(1)} + R_{2G} V_{2G}(-\theta_g) + R_{1P} V_{1P}(-\theta_g) , \\ R_{1P} &= R_{1P}^{(1)} + R_{2G} V_{2G} \left( -\frac{\pi}{2} \right) + R_{1P} V_{1P} \left( -\frac{\pi}{2} \right) , \text{ and} \\ R_{2G} &= R_{2G}^{(1)} + R_{1G} V_{1G}(\pi - \theta_g) , \end{aligned}$$

where the quantities  $V_{1G}$ ,  $V_{1P}$ , and  $V_{2G}$  are the unit-wave diffractions used in Eqs. (6) and (13).

The total diffracted wave from the aperture may be expressed as the superposition of the total diffracted rays from edges 1 and 2 plus the total reflected ray to yield

$$(19) \quad \begin{aligned} R_T(\theta) &= R_1(\theta) + R_2(\theta) e^{jkh \cos(\theta + \theta_g)} \\ &\quad + R_1(-\theta) e^{-j2ka \sin \theta} . \end{aligned}$$

Each term in Eq. (19) contributes to the radiation pattern only in certain regions as follows:

$$(20) \quad \begin{aligned} R_1(\theta): & \quad -\theta_g < \theta < \pi - WA_1 , \\ R_2(\theta): & \quad -\pi + WA_2 < \theta < \pi - \theta_g , \text{ and} \\ R_1(-\theta): & \quad \theta_g < \theta < \frac{\pi}{2} . \end{aligned}$$

The exponential factors refer each term to a common phase reference at edge 1.

For the case in which  $\theta_g = 90^\circ$ , no reflected rays contribute to the radiation pattern and

$$(21) \quad R_{1P} = 0, \text{ for } \theta_g = 90^\circ .$$

In this case there are only two unknown rays  $R_{1G}$  and  $R_{2G}$ ; and the simultaneous equations are

$$(22) \quad \theta_g = 90^\circ: ,$$

$$R_{1G} = R_{1G}^{(1)} + R_{2G} V_{2G} \left( -\frac{\pi}{2} \right) , \text{ and}$$

$$R_{2G} = R_{2G}^{(1)} + R_{1G} V_{1G} \left( \frac{\pi}{2} \right) .$$

The total radiation pattern for the  $\theta_g = 90^\circ$  case is given by

$$(23) \quad \theta_g = 90^\circ:$$

$$R_T(\theta) = R_1(\theta) + R_2(\theta) e^{-jka \sin \theta} ,$$

where the appropriate regions for the respective terms are

$$(24) \quad R_1(\theta): \quad -\frac{\pi}{2} < \theta < \pi$$

and

$$R_2(\theta): \quad -\pi < \theta < \frac{\pi}{2} .$$

### B. TE<sub>01</sub> Mode

The diffraction at the aperture of the parallel-plate waveguide may be treated for the TE<sub>01</sub> mode in a similar manner as was the TEM mode. For the TE<sub>01</sub> case the electric field is the component perpendicular to the plane of Fig. 2 and thus the fields are transverse electric (TE) everywhere. The incident mode in the guide may be represented by a plane wave reflecting between the guide walls as shown in Fig. 2.

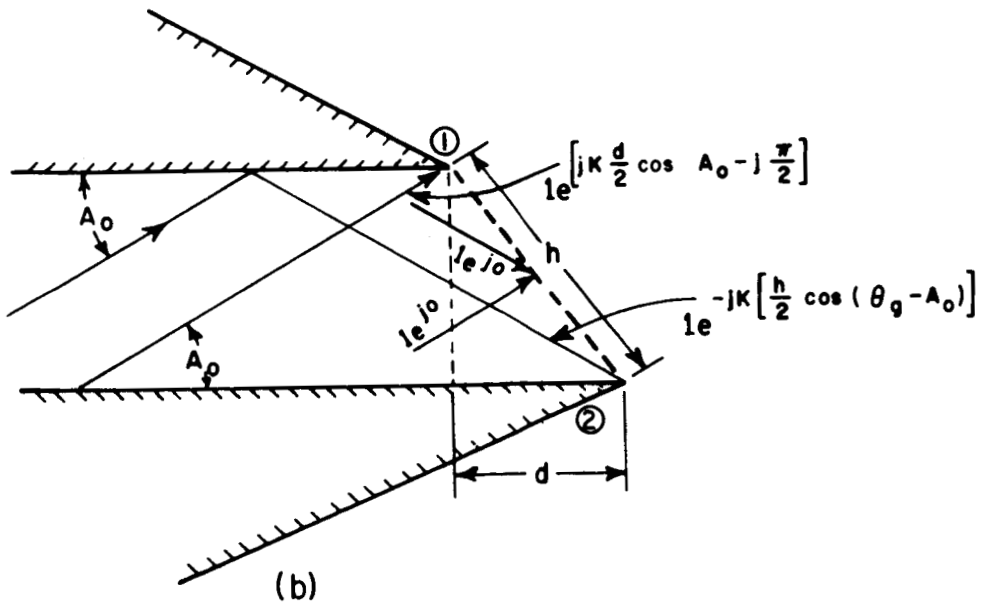
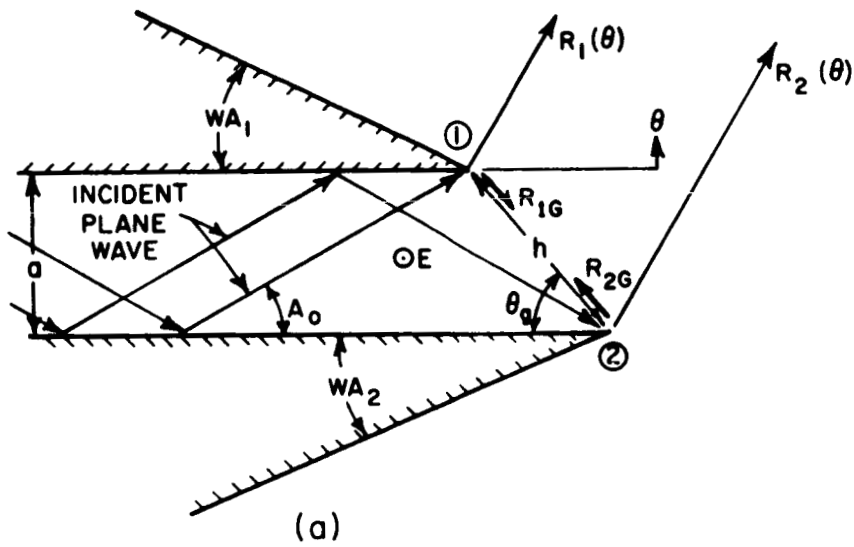


Fig. 2.  $TE_{01}$  mode in a parallel-plate waveguide.

The angle  $A_0$  of reflection between the walls is given by

$$(25) \quad A_0 = \sin^{-1} \frac{\lambda}{2a} ,$$

where  $a$  is the guide width.

The resulting modal distribution is sinusoidal across the guide cross section with an incident power flow of

$$(26) \quad P_0 = 2 a Y_0 \cos A_0, \quad Y_0 = \sqrt{\epsilon_0 / \mu_0} .$$

For Eq. (26) the incident wave is assumed to have unit-amplitude electric field in each of its two plane wave components. The associated modal voltage is

$$(27) \quad V_0 = \sqrt{2a \frac{Y_0}{Y_g} \cos A_0} ,$$

where  $Y_g$  is the characteristic admittance of the  $TE_{01}$  mode.

Examination of Fig. 2 reveals that two cases must be distinguished in analyzing the fields, as determined by

$$\text{Case I: } A_0 > \theta_g ,$$

and

$$\text{Case II: } A_0 \leq \theta_g .$$

Case I corresponds to the situation in which edge 2 is not illuminated by the incident plane wave. Thus, for Case I no singly diffracted ray emanates from edge 2. For Case II both edges are illuminated by the incident wave hence singly diffracted rays emanate from both edges.

Since the electric field is polarized parallel to the edges of the wedges for the  $TE_{01}$  mode, it is representable by a scalar function. The singly diffracted ray from edge 1 with the incident wave phase reference at the aperture center is

$$(28) \quad R_1^{(1)}(\theta) = \frac{1}{n_1} \sin \frac{\pi}{n_1} \left[ \frac{1}{\cos \frac{\pi}{n_1} - \cos \frac{\pi + \theta - A_0}{n_1}} - \frac{1}{\cos \frac{\pi}{n_1} - \cos \frac{\pi + \theta + A_0}{n_1}} \right] e^{jk \frac{d}{2} \cos A_0 - j \frac{\pi}{2}}$$

where the exponential factor represents the phase of the incident plane wave at edge 1. It should be noted that  $R_1^{(1)}(\theta)$  and all other diffracted rays represent waves that appear to emanate from the edges where diffraction took place.

For Case II ( $A_0 \leq \theta_g$ ) the singly diffracted ray from edge 2 is given by

$$(29) \quad R_2^{(1)}(\theta) = \frac{1}{n_2} \sin \frac{\pi}{n_2} e^{-jk \frac{h}{2} \cos(\theta_g - A_0)} \left[ \frac{1}{\cos \frac{\pi}{n_2} - \cos \frac{\pi - \theta - A_0}{n_2}} - \frac{1}{\cos \frac{\pi}{n_2} - \cos \frac{\pi - \theta + A_0}{n_2}} \right]$$

where the exponential factor represents the phase of the incident plane wave at edge 2. The first-order reflected rays are given by

$$(30) \quad R_{RFL}(\theta) = -R_1^{(1)}(-\theta), \quad \theta_g < \theta < \frac{\pi}{2}$$

where the preceding minus sign results from the reflection.

Multiple diffractions occur in the same manner for the  $TE_{01}$  mode as for the TEM mode but with its appropriate diffraction formula. Thus the total higher-order diffracted waves from edges 1 and 2 for the  $TE_{01}$  mode are given by

$$(31) \quad R_1^{(h)}(\theta) = R_2G[V_B(h, \theta + \theta_g) - V_B(h, 2\pi + \theta - \theta_g)] \\ - R_1P \left[ V_B\left(2a, \frac{\pi}{2} + \theta\right) - V_B\left(2a, \frac{3\pi}{2} + \theta\right) \right]$$

and

$$(32) \quad R_2^{(h)}(\theta) = R_1G[V_B(h, \pi - \theta - \theta_g) - V_B(h, \pi - \theta + \theta_g)] .$$

The total wave from each edge is obtained by using the  $TE_{01}$  rays in the same equations valid for the TEM mode; i.e., Eqs. (10) and (17) through (24). The unknown illuminating rays are determined in the same manner as with the TEM mode by using the formulations for  $R_1^{(1)}$ ,  $R_2^{(1)}$ ,  $R_1^{(h)}$ , and  $R_2^{(h)}$  given above for the  $TE_{01}$  mode.

It should be noted that this analysis is approximate insofar as the second- and higher-order diffractions are approximated by wedge diffractions resulting from uniform cylindrical wave incidence. Thus the accuracy of the results is governed by the similarity that each diffracted wave has to a uniform cylindrical wave in the vicinity of the edge which it illuminates. In general each diffracted wave approximates a uniform cylindrical wave if viewed sufficiently far from any shadow boundary that results from its source. Thus multiple diffractions may be analyzed in such cases by assuming cylindrical wave diffraction. A criterion for the validity of the cylindrical wave approximation can be based on the characteristics of the  $V_B(r, \phi)$  function. For values of  $r(1 + \cos \phi)$  greater than a certain magnitude the  $V_B$  function takes on the characteristics of a cylindrical wave radiating from the edge. If this criterion is satisfied for values of  $r$  and  $\phi$  which correspond to another edge at which a subsequent diffraction takes place, then the assumption of cylindrical wave incidence is valid. Values of  $r(1 + \cos \phi)$  greater than one wavelength are quite adequate for this purpose, and fairly good results can be obtained for values as low as  $\lambda/4$ . In the case of the  $\theta_g = 90^\circ$  guide, for example, the singly diffracted wave from each edge has a value of  $\phi = 90^\circ$  which corresponds to the direction of the opposite edge. Thus the doubly diffracted waves may be adequately treated as those of cylindrical wave illumination for guide widths (which correspond to  $r$  for this case) down to about  $\lambda/4$ . However, each doubly diffracted wave has a shadow boundary for its reflected component which coincides with the opposite edge; e.g.,  $R_1^{(2)}(\theta)$  has a reflection boundary at  $\theta = -\pi/2$ , corresponding to the direction of edge 2. Hence the triply diffracted wave  $R_2^{(3)}$  which

results from the illumination of edge 2 by the doubly diffracted wave  $R_1^{(2)}$  is not accurately given for the  $\theta_g = 90^\circ$  case by assuming  $R_1^{(2)}$  to be a cylindrical wave radiating from edge 1.

Consequently, the use of cylindrical wave diffraction is not very accurate for third- and higher-orders of diffraction in the  $\theta_g = 90^\circ$  case. Moreover, the use of only the first two orders (singly and doubly diffracted waves) is quite accurate over most of the pattern, except in the vicinity of  $\theta = \pm 90^\circ$  for guide widths less than a wavelength. For other guide angles (i.e.,  $\theta_g < 90^\circ$ ) the use of higher-order diffraction is more accurate.

### III. EFFECTIVE APERTURE

#### A. TEM Mode

In the derivation of the formulation for the reflection coefficient the effective aperture of the guide for plane wave incidence is used. The modal current induced in a guide by an incident plane wave may readily be derived in terms of the more general case of an incident cylindrical wave. The modal current induced in a guide by a line source may be obtained by reciprocity, as illustrated in Fig. 3. The modal

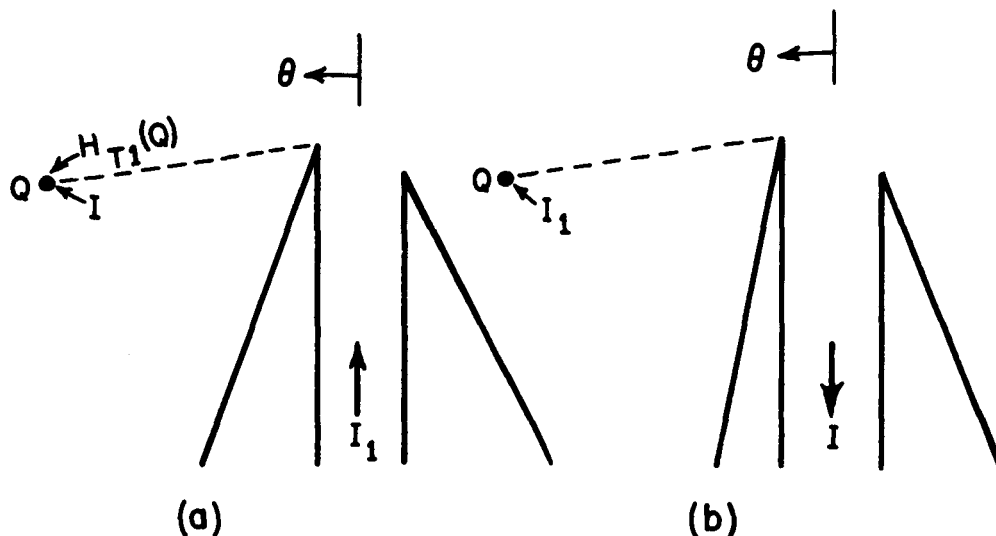


Fig. 3. Use of reciprocity to obtain the response of a guide to a line source.

current induced in the line source by the guide with modal current excitation  $I_1$  is first obtained. The power received by the line source is the product of the effective aperture of the line source,  $\lambda/2\pi$ , and the power density, and is given by

$$(33) \quad P = \frac{\lambda}{2\pi} |H_{T1}(Q)|^2 Z_0,$$

where  $H_{T1}$  is the field of the guide at point Q as shown in Fig. 3a. The modal current received by the line source is thus given by

$$(34) \quad I = \sqrt{\frac{\lambda}{2\pi a}} H_T(Q) I_1,$$

where  $H_T(Q)$  is the field at point Q for an incident wave in the guide of unit-amplitude magnetic field; and hence the associated modal current of the incident mode is  $\sqrt{a}$ . By reciprocity, current I is the modal current induced in the guide by the line source excited by a modal current  $I_1$ .

If the line source is located in the far-field region of the guide, the ray form given in Eq. (1) may be used. Then

$$(35) \quad I = \sqrt{\frac{\lambda}{2\pi a}} D_T I_1 \frac{e^{-jkr}}{\sqrt{r}}.$$

But the field at the guide aperture which is attributed to the line source is given by

$$(36) \quad H^i = I_1 \frac{e^{-j\left(kr - \frac{\pi}{4}\right)}}{\sqrt{2\pi r}}.$$

Thus the modal current induced by an incident cylindrical wave with its source in the far field of the guide is given by

$$(37) \quad I = \sqrt{\frac{\lambda}{a}} D_T H_i e^{-j\frac{\pi}{4}},$$

where  $H^i$  is the incident field at the guide aperture. Equation (37) is also applicable for an incident plane wave. For grazing incidence along the

surface of the guide as employed in the derivation of reflection coefficient, the concept of the incident field must be properly interpreted. For grazing incidence, one-half of the field incident along the surface of the guide must be treated as the incident field and the other half as the reflected field. This may be seen from Fig. 4 in which the magnetic line source is located on an infinite ground plane. For non-grazing incidence, as shown in Fig. 4a, the effective aperture of the line source is  $\lambda/\pi$ . If the effective aperture for grazing incidence is defined as  $\lambda/\pi$ , then the incident field intensity  $H^i$  must be taken as one-half of the total field  $H^t$  incident on the line source; the other half must be considered as the reflected field  $H^r$ , as shown in Fig. 4b.

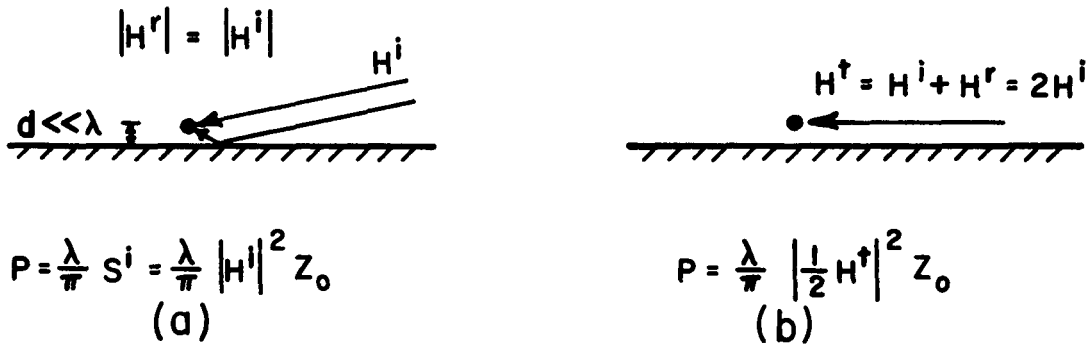


Fig. 4. Effective aperture of a line source on a ground plane.

### B. TE<sub>01</sub> Mode

Reciprocity is again applied to obtain the TE<sub>01</sub> response of a guide to a line source. The modal voltage received by the line source with characteristic admittance  $Y_0$  in Fig. 5a is given by

$$(38) \quad V_R = \sqrt{\frac{\lambda}{2\pi}} E_T(Q) .$$

$E_T(Q)$  is the field at point Q due to the guide with a modal voltage excitation given by Eq. (27) as

$$(39) \quad V_T = \sqrt{2a \frac{Y_0}{Y_g} \cos A_0} ,$$

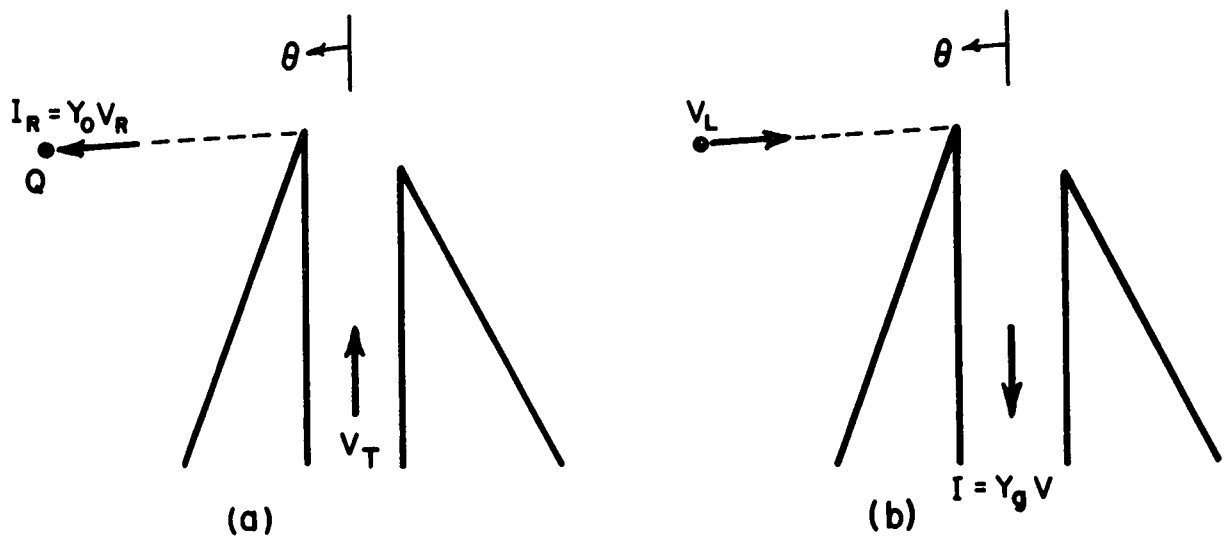


Fig. 5. Response of the TE<sub>01</sub> receiving guide to the equivalent line source.

and phase-referenced to the guide aperture center. The modal current  $I$  induced in the guide by the line source, as shown in Fig. 5b is given by reciprocity<sup>4</sup> as

$$(40) \quad I = \frac{V_L}{V_T} I_R,$$

where  $V_L$  is the modal voltage of the line source. The field  $E^i$  of the line source incident upon the guide aperture may be written in terms of the modal voltage  $V_L$  as

$$(41) \quad E^i = V_L \frac{e^{-j\left(kr - \frac{\pi}{4}\right)}}{\sqrt{2\pi r}}.$$

If the line source is located in the far-field region of the guide, the ray form of the field  $E_T(Q)$  may be used in Eq. (38); this gives

$$(42) \quad I_R = Y_0 V_R = \sqrt{\frac{\lambda}{2\pi}} Y_0 D_T(\theta) \frac{e^{-jkr}}{\sqrt{r}},$$

where  $D_T(\theta)$  is the diffraction coefficient of the guide in the direction of the line source with its phase referenced at the guide aperture center. Using Eqs. (39), (41), and (42) in Eq. (40), the modal voltage induced in the guide by an incident cylindrical wave may be written as

$$(43) \quad V = \frac{I}{Y_g} = \sqrt{\frac{Y_0}{Y_g}} \frac{\sqrt{\lambda} e^{-j\frac{\pi}{4}}}{\sqrt{2a \cos A_0}} D_T(\theta) E^i,$$

where  $E^i$  is the incident field at the guide aperture center.

#### IV. REFLECTION COEFFICIENT OF APERTURE

##### A. TEM Mode

The reflection coefficient of the parallel-plate guide aperture can be analyzed by identifying the two situations shown in Fig. 6. Because of the symmetry of half-plane diffraction, the diffracted field distributions of (a) and (b) are identical except for sign. Thus the power reflected back into the guide by mismatch at the aperture (a) is the same as that received by the guide from the plane waves incident outside the guide (b). The modal current of (a) is the negative of that of (b).

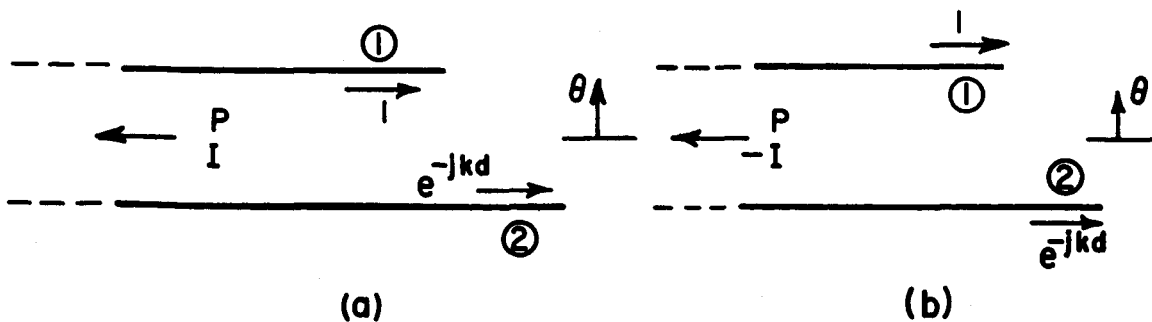


Fig. 6. Incident plane wave cases.

The modal current induced in the guide by the two incident plane waves as shown in Fig. 6b is given by the use of Eq. (37). For the plane wave incident upon edge 1 in (b) the total diffraction coefficient is given by

$$(44) \quad D_1(\psi = 2\pi) = \frac{e^{-j\frac{\pi}{4}}}{\sqrt{2\pi k}} R_1(\theta = \pi) \quad ,$$

where  $R_1$  is obtained from Eq. (17). Because the plane wave has grazing incidence the incident field of Eq. (37) must be taken as one-half of that shown in Fig. 6b. Thus the modal current induced by the plane wave incident on edge 1 is given by

$$(45) \quad I_1 = \frac{1}{2} \sqrt{\frac{\lambda}{a}} D_1(\psi = 2\pi) e^{-j\frac{\pi}{4}} \quad .$$

The modal current induced by the plane wave incident on edge 2 is derived in the same manner, giving

$$(46) \quad I_2 = \frac{1}{2} e^{-jkd} \sqrt{\frac{\lambda}{a}} D_2(\psi = 2\pi) e^{-j\frac{\pi}{4}} \quad ,$$

where  $1/2 e^{-jkd}$  is the incident field of the incident wave at edge 2. By superposition the total modal current ( $-I$ ) induced in the guide of (b) is given by

$$(47) \quad -I = I_1 + I_2 = \frac{1}{2} \sqrt{\frac{\lambda}{a}} [D_1(\psi = 2\pi) + e^{-jkd} D_2(\psi = 2\pi)] e^{-j\frac{\pi}{4}} \quad .$$

The modal current  $I$  of the reflected wave of (a) may be written in a form which yields a direct physical interpretation; i.e.,

$$(48) \quad I = \frac{1}{2} \sqrt{\frac{\lambda}{a}} [D_1(\psi = 0) + e^{-jkd} D_2(\psi = 0)] e^{-j\frac{\pi}{4}}$$

$$= \frac{1}{2k\sqrt{a}} [R_1(\theta = -\pi) + e^{-jkd} R_2(\theta = \pi)] e^{-j\frac{\pi}{2}}$$

In Eq. (48) the modal current of the reflected wave is obtained in terms of the rays diffracted back along the inside instead of the outside of the waveguide walls. In fact Eq. (48) gives the same result as is obtained directly from Eq. (37) by assuming that Eq. (37) is valid for a plane wave incident within the guide.

The TEM reflection coefficient of the parallel-plate waveguide aperture with phase referred to edge 1 is thus given by

$$(49) \quad \Gamma = \frac{I}{I_0} = \frac{1}{2} \frac{\sqrt{\lambda}}{a} [D_1(\psi = 0) + e^{-jkd} D_2(\psi = 0)] e^{-j \frac{\pi}{4}},$$

where  $D_1(\psi = 0)$  and  $D_2(\psi = 0)$  are the total diffraction coefficients for edges 1 and 2 corresponding to the rays diffracted back along the inside of the waveguide walls.

The derivation of Eq. (49) is valid only for thin-walled guides (zero wedge angles). However, the physical interpretation that the reflection coefficient is given by the diffraction coefficients along the inside of the guide walls suggests that the formula may be applicable to waveguides with walls formed from non-zero angle wedges. By comparison with measurements and other methods of analysis the formula of Eq. (49) has been shown to give correct results for reflection coefficient of guides with 90° wedge angles; this comparison is given in the section on results. Equation (49) is believed to be valid for all wedge angles. It should be noted that the reflection coefficient defined by Eq. (49) is in terms of magnetic fields, and hence differs by a minus sign from the normal transmission line definition of voltage reflection coefficient.

### B. TE<sub>01</sub> Mode

The reflection coefficient of the parallel-plate waveguide for the TE<sub>01</sub> mode may be analogously derived as was that for the TEM mode. Again because of the symmetry of half-plane diffraction, the diffracted field distribution of Fig. 7a and b are identical because for zero wedge angle

$$(50) \quad V_B(r, \theta - A_0) - V_B(r, \theta + A_0) = V_B(r, \theta + A_0 - 2\pi) - V_B(r, \theta + 2\pi - A_0).$$

Equation (43) is used to obtain the modal voltage induced in the guide by the two incident plane waves of Fig. 7b.

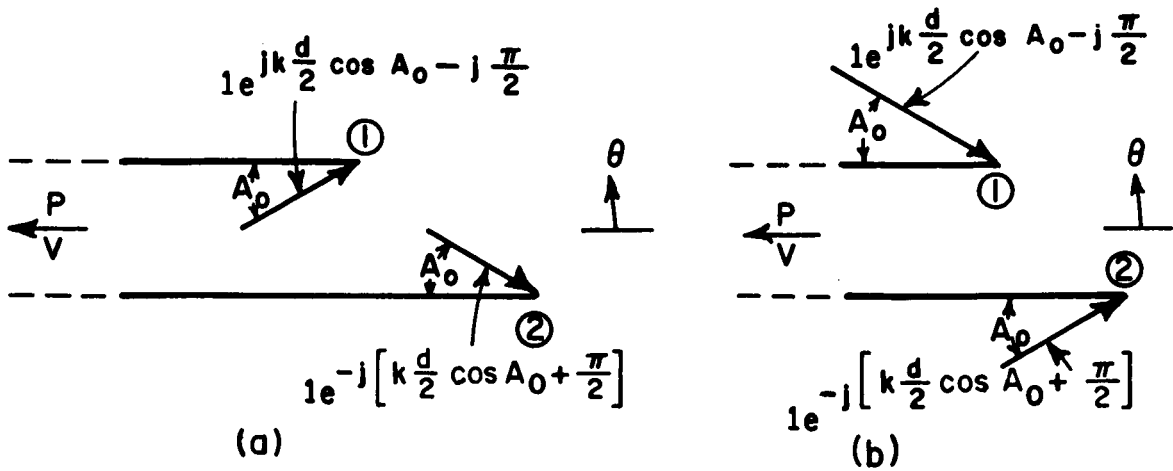


Fig. 7. Incident plane wave case,  $TE_{01}$  mode.

For the plane wave incident on edge 1 in Fig. 7b the total diffraction coefficient is given by

$$(51) \quad D_1(\psi = 2\pi - A_0) = \frac{e^{-j \frac{\pi}{4}}}{\sqrt{2\pi k}} R_1(\theta = \pi - A_0) ,$$

where  $R_1$  is obtained from Eq. (17) for the  $TE_{01}$  mode. The modal voltage induced by the plane wave incident on edge 1 in Fig. 7b is given by Eq. (43) by

$$(52) \quad V_1 = \sqrt{\frac{Y_0}{Y_g}} \sqrt{\lambda} \frac{e^{-j \frac{\pi}{4}}}{\sqrt{2a \cos A_0}} D_1(\psi = 2\pi - A_0) \\ \times e^{+j \left[ k \frac{h}{2} \sin \theta_g \cos A_0 - \frac{\pi}{2} \right]} ,$$

where the phase term results from referring the incident plane wave to the guide aperture center. The modal voltage induced by the plane wave incident on edge 2 is similarly given by

$$(53) \quad V_2 = \sqrt{\frac{Y_0}{Y_g}} \frac{\sqrt{\lambda} e^{-j\frac{\pi}{4}}}{\sqrt{2a \cos A_0}} D_2(\psi = 2\pi - A_0) \\ \times e^{-j \left[ k \frac{h}{2} \sin \theta_g \cos A_0 + \frac{\pi}{2} \right]}$$

The total modal voltage,  $V$ , induced in the guide is given by

$$(54) \quad V = V_1 + V_2 = \sqrt{\frac{Y_0}{Y_g}} \frac{\sqrt{\lambda} e^{-j\frac{\pi}{4}}}{\sqrt{2a \cos A_0}} \\ \times \left\{ D_1(\psi = 2\pi - A_0) e^{j \left[ k \frac{h}{2} \sin \theta_g \cos A_0 - \frac{\pi}{2} \right]} \right. \\ \left. + D_2(\psi = 2\pi - A_0) e^{-j \left[ k \frac{h}{2} \sin \theta_g \cos A_0 + \frac{\pi}{2} \right]} \right\} ; \\ V = \sqrt{\frac{Y_0}{Y_g}} \frac{-1}{2\pi \sqrt{2a \cos A_0}} \left\{ R_1(\theta = \pi - A_0) e^{j \left[ k \frac{h}{2} \sin \theta_g \cos A_0 \right]} \right. \\ \left. + R_2(\theta = A_0 - \pi) e^{-j \left[ k \frac{h}{2} \sin \theta_g \cos A_0 \right]} \right\} .$$

The  $TE_{01}$  reflection coefficient of the parallel-plate waveguide aperture with phase referred to aperture center is thus obtained from Eqs. (40) and (54) as

$$(55) \quad \Gamma = \frac{V}{V_0} = \frac{\sqrt{\lambda} e^{-j\frac{3\pi}{4}}}{2a \cos A_0} \\ \left\{ D_1 \left( \begin{array}{l} \theta = A_0 - \pi \\ \psi = A_0 \end{array} \right) e^{j k \left[ \frac{h}{2} \sin \theta_g \cos A_0 \right]} \right. \\ \left. + D_2 \left( \begin{array}{l} \theta = \pi - A_0 \\ \psi = A_0 \end{array} \right) e^{-j \left[ k \frac{h}{2} \sin \theta_g \cos A_0 \right]} \right\} ,$$

where  $D_1(\theta = A_0 - \pi)$  and  $D_2(\theta = \pi - A_0)$  are the total diffraction coefficients for edges 1 and 2 with phase referred to aperture center corresponding to the rays diffracted back into the waveguide. The same physical interpretation concerning non-zero wedge angles is applied for the  $TE_{01}$

mode as was the TEM mode. Consequently, Eq. (55) is also believed general for all wedge angles.

## V. NUMERICAL RESULTS

### A. TEM Mode

The TEM reflection coefficient of the parallel plate waveguide was calculated as a function of guide width with the aid of two SCATRAN programs on the IBM 7094 digital computer. Two principal wedge angles ( $0^\circ$  and  $90^\circ$ ) were considered although this analysis may be applied to any other wedge angles. Two methods were used to compute the reflection coefficient; i.e., Double-Diffraction and Higher-Order Concept. The Double-Diffraction method considers only up to second-order diffraction terms, while the Higher-Order method employs the simultaneous equation solution of higher-order diffraction contributions.

Experimental verification for the TEM reflection coefficient were obtained with the aid of a slotted sectoral horn, as shown in Fig. 8. The horn, with its large width at the aperture and small flare angle, adequately simulates an infinite parallel-plate waveguide. The standing-wave was measured along the slot in the "parallel-plate" sector of the horn. To measure reflection coefficient at the aperture, however, the flare angle of the horn must be taken into account because of the sectoral divergence of energy along the axis of the horn.

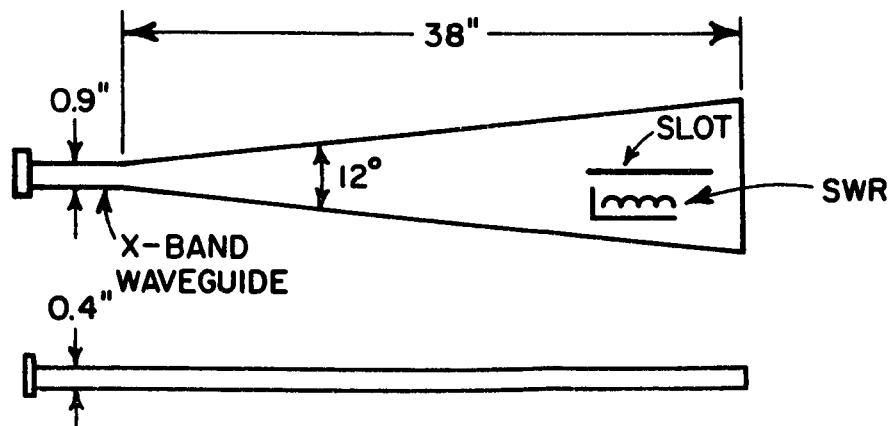


Fig. 8. TEM sectoral horn.

The envelope of the SWR curve was measured by plotting the SWR minima and maxima as a function of position along the slot. By extending the measured SWR envelope to the aperture, the aperture reflection coefficient of the parallel-plate waveguide was obtained. Guide width variations were obtained by varying the frequency of operation.

Other forms of analysis for the reflection coefficient were also calculated as verifications. They are: for the half-plane guide, Noble (Wiener-Hopf technique);<sup>5</sup> for the 90° wedge angle guide, Compton and Harrington<sup>6,7</sup> and Do Amaral and Bautista Vidal.<sup>8,9</sup> The results for the TEM reflection coefficient are shown in Figs. 9 through 19.

Figure 9 shows the Double-Diffraction method reflection coefficient magnitudes for the half-plane guide (WA = 0°) with  $\theta_g = 30^\circ$ ,  $60^\circ$ , and  $90^\circ$ . The reflection coefficient as a function of guide width is seen to become oscillatory as the guide truncation angle  $\theta_g$  is decreased.

Figures 10 through 15 compare the Double Diffraction and Higher-Order methods. The reflection coefficient magnitudes for the half-plane guides,  $\theta_g = 90^\circ$ , case are presented in Fig. 10 with the experimentally measured results and the values computed by the Weiner-Hopf technique.<sup>5</sup> Because of the previously mentioned shadow boundaries the Higher-Order method results are seen to be less accurate than the Double-Diffraction Method. Figure 11 shows the computed reflection coefficient phase for the same guides. Figures 12 and 13 show the results for  $\theta_g = 60^\circ$ . The measured reflection coefficient magnitudes are shown in the same comparison for  $\theta_g = 30^\circ$  in Fig. 14. Because the reflection coefficients in question are quite low, absolute levels become difficult to measure, but the same trends are nevertheless observed for both the measured and calculated results. Figure 15 presents the comparison in reflection coefficient phase for double - versus higher-order diffraction.

Figure 16 shows the reflection coefficient magnitudes computed by the Double-Diffraction Method for WA = 0° and 90°. Experimental results for both cases are presented along with analytical results obtained from Compton and Harrington<sup>6,7</sup> and Do Amaral and Bautista Vidal<sup>8</sup> for the WA = 90° case. Figure 17 presents the corresponding phase comparison. Figures 18 and 19 show the reflection coefficients of ground-plane mounted guides with truncation angles of 30°, 60°, and 90°.

## B. TE<sub>01</sub> Mode

Double-Diffraction and Higher-Order Methods are used in calculating the TE<sub>01</sub> reflection coefficient. The Scatran computer programs used were similar to those used for the TEM mode except for changes in the appropriate diffraction functions. The calculated results are plotted in Figs. 20-22 with Wiener-Hopf technique results<sup>10</sup> for a half-plane guide with 90° truncation angle. Figures 23 and 24 show the calculated reflection coefficients for ground-plane mounted guides compared with the variational solution from Harrington.<sup>11</sup>

## VI. CONCLUSIONS

The reflection coefficient of the parallel-plate waveguide aperture is analyzed by wedge diffraction techniques for both TEM and TE<sub>01</sub> modes. Upon comparison with calculations from other analyses the accuracy of this method is found to be generally quite good. This method agrees quite well with the Wiener-Hopf method which gives the exact solution for the normally truncated, thin-walled guide. Close agreement with variational analyses is obtained for the normally truncated guide mounted in a ground plane.

Numerical results are given for a number of cases from which the influence of guide width, truncation angle, and wedge angles is seen. The reflection coefficient generally decreases as a function of increasing guide width, although truncation angles may introduce oscillations in the curve. Furthermore, truncation angles different from normal usually produce lower reflection coefficient levels than does normal truncation.

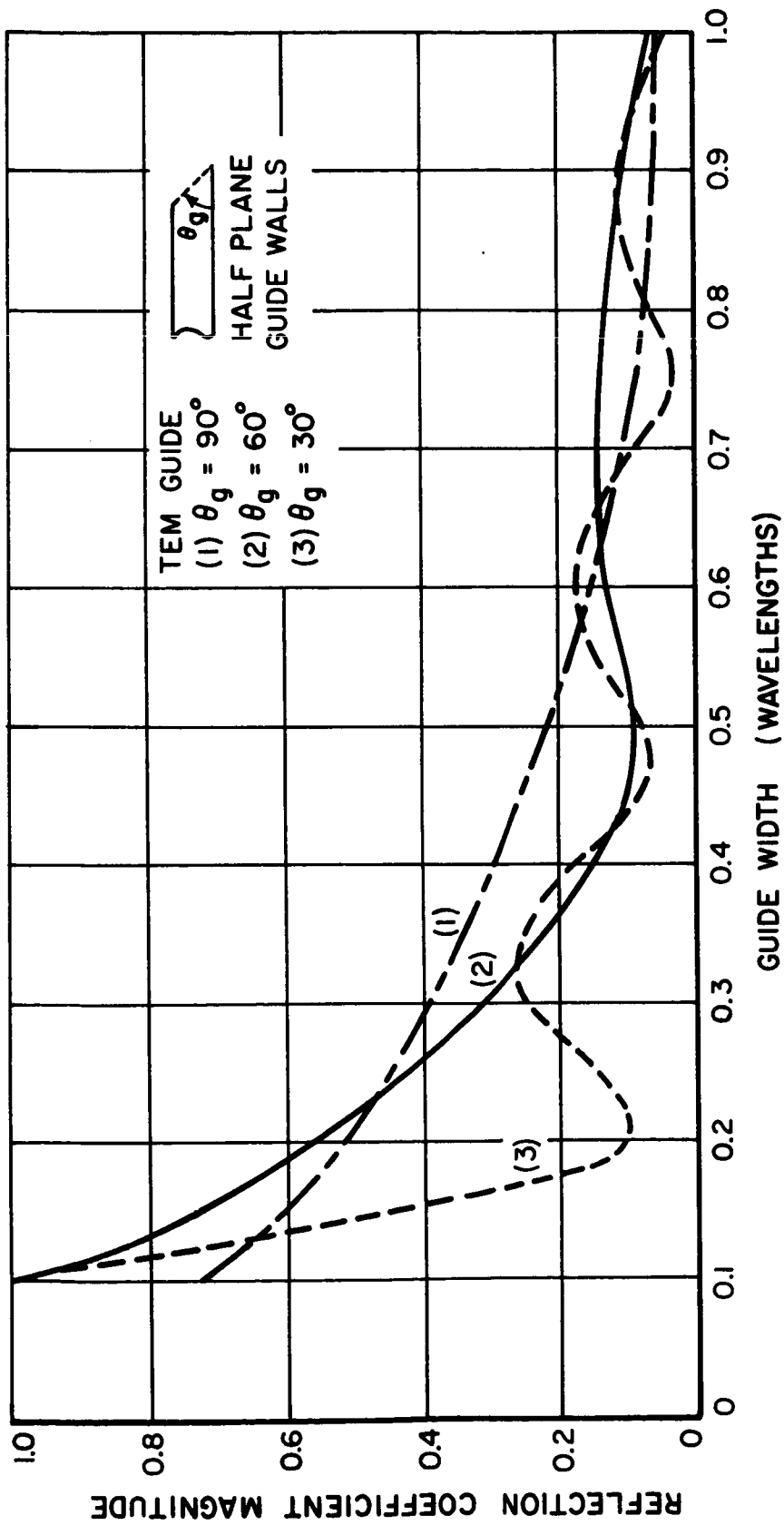


Fig. 9. TEM reflection coefficient magnitudes for half-plane guides by the double-diffraction method.

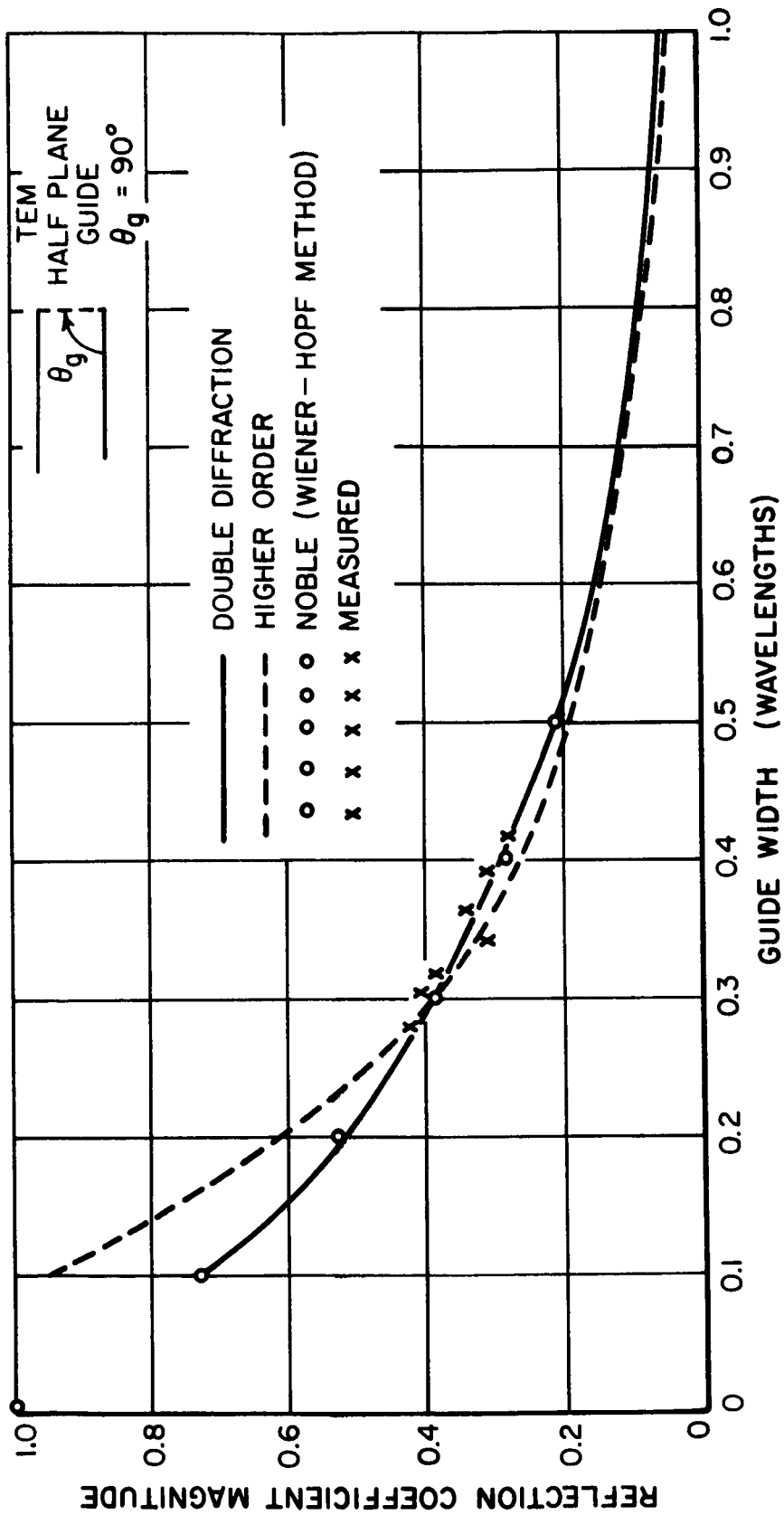


Fig. 10. TEM reflection coefficient magnitudes for a normally truncated half-plane guide.

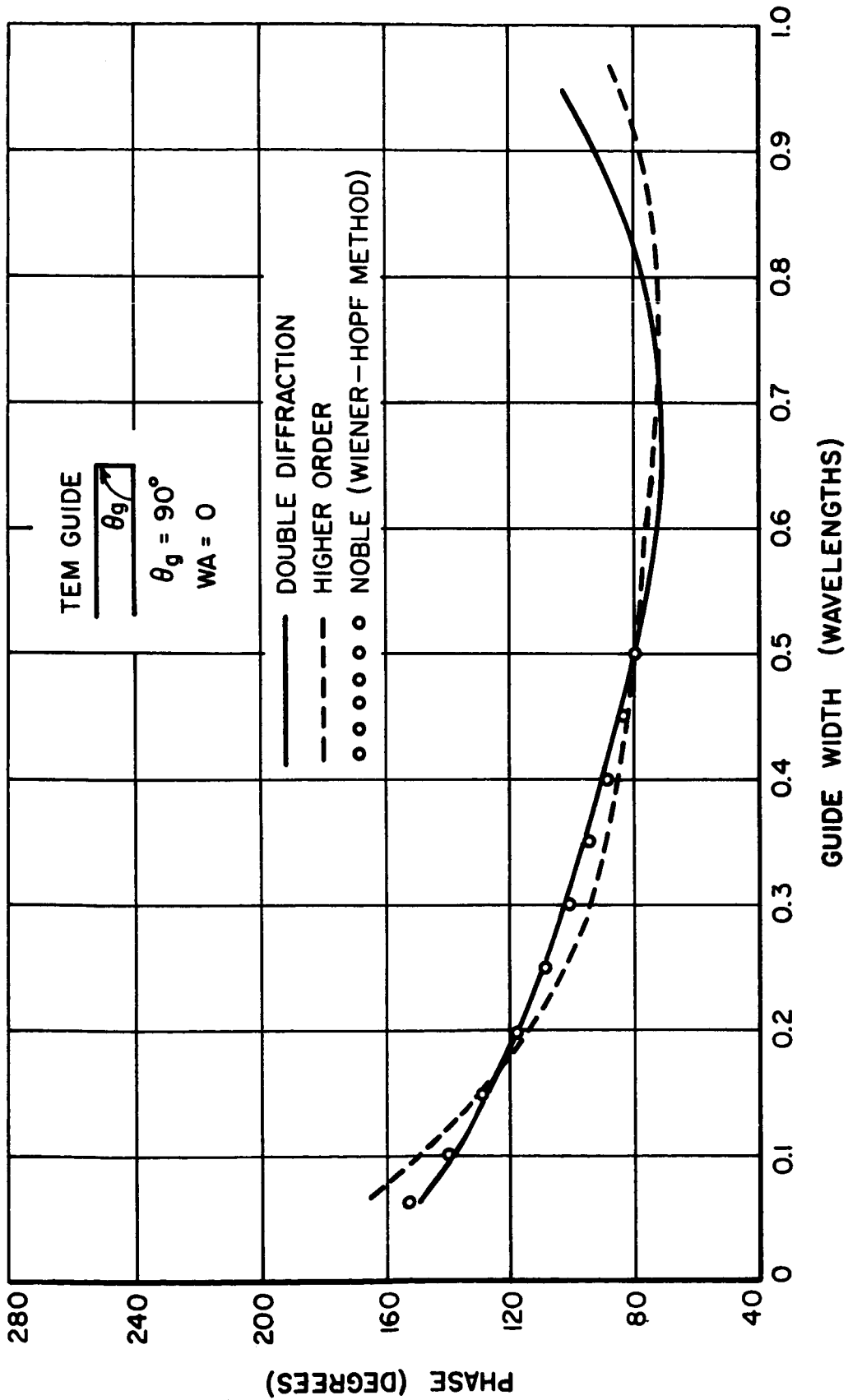


Fig. 11. TEM reflection coefficient phase for a normally truncated half-plane guide.

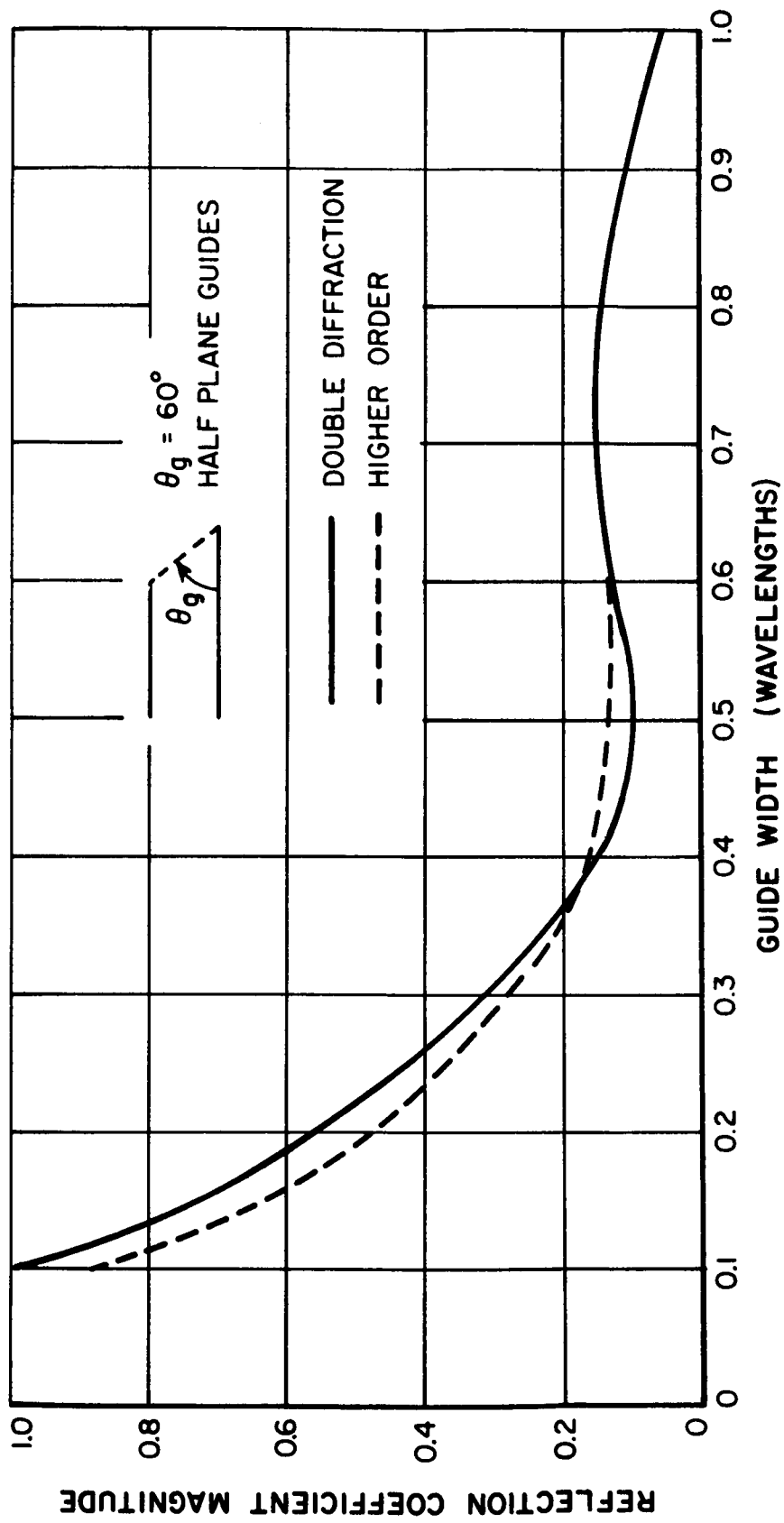


Fig. 12. TEM reflection coefficient magnitude ( $\theta_g = 60^\circ$ ).

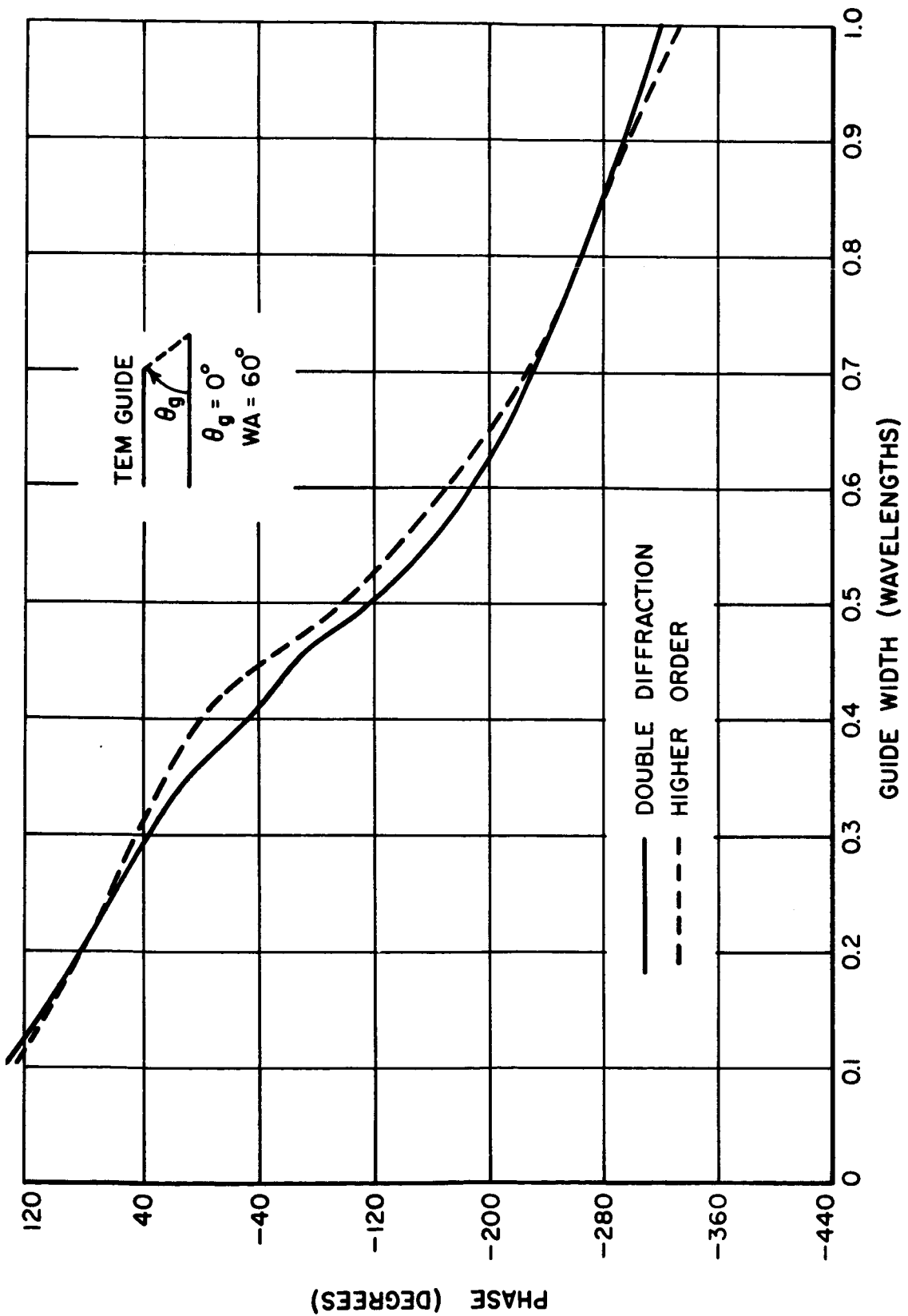


Fig. 13 TEM reflection coefficient phase ( $\theta_g = 60^\circ$ ).

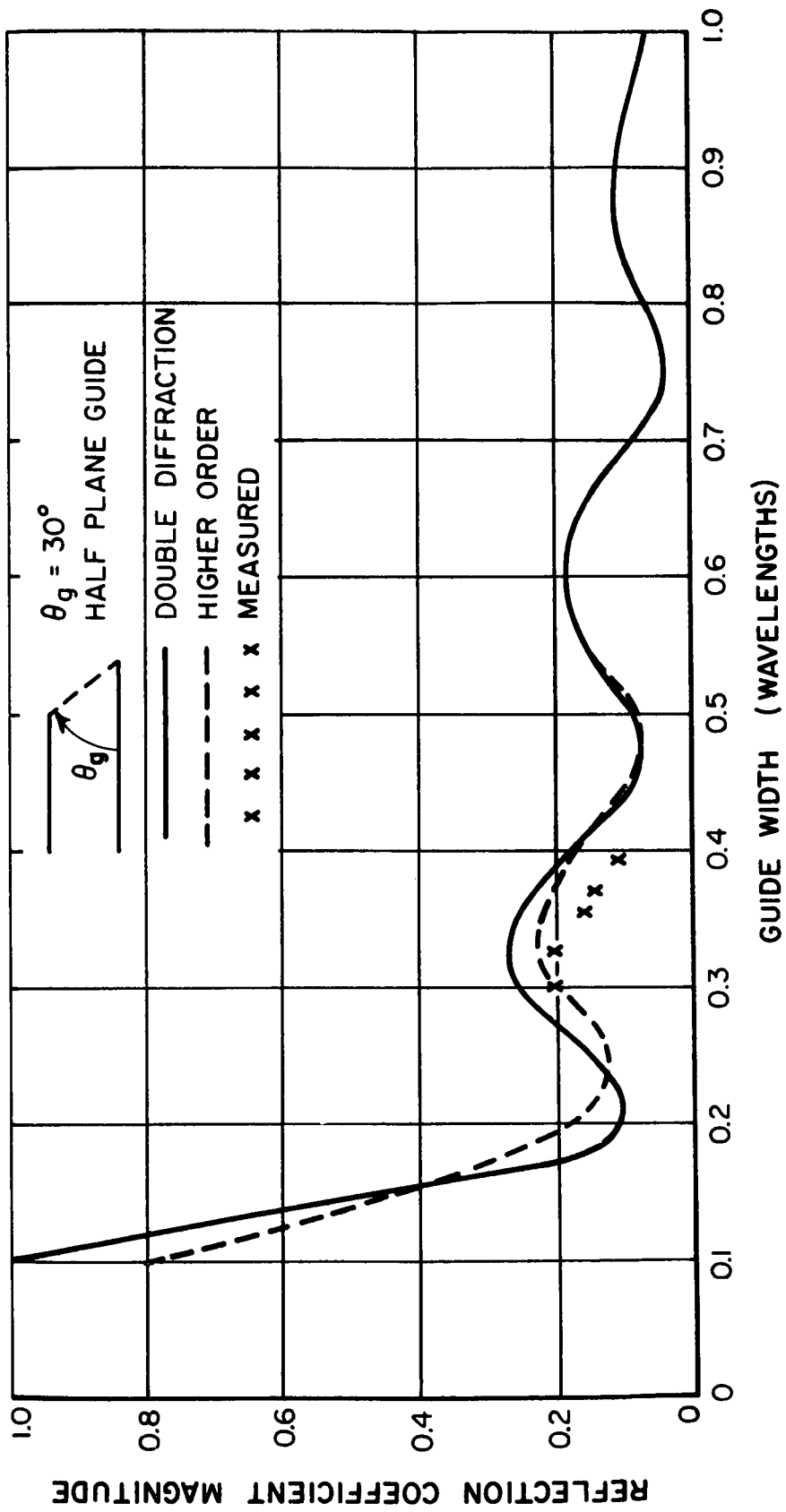


Fig. 14. TEM reflection coefficient magnitude ( $\theta_g = 30^\circ$ ).

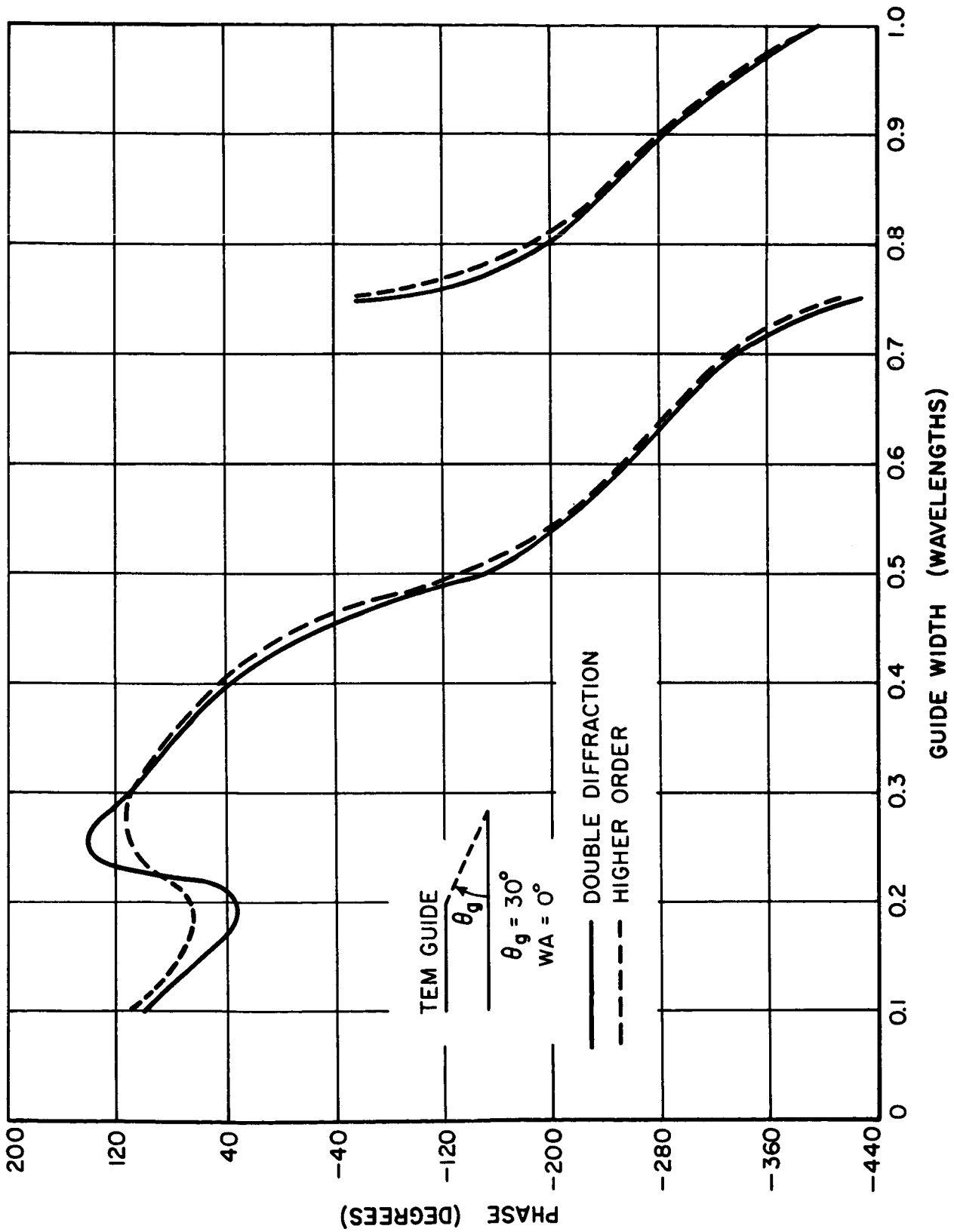


Fig. 15. TEM reflection coefficient phase ( $\theta_g = 30^\circ$ ).

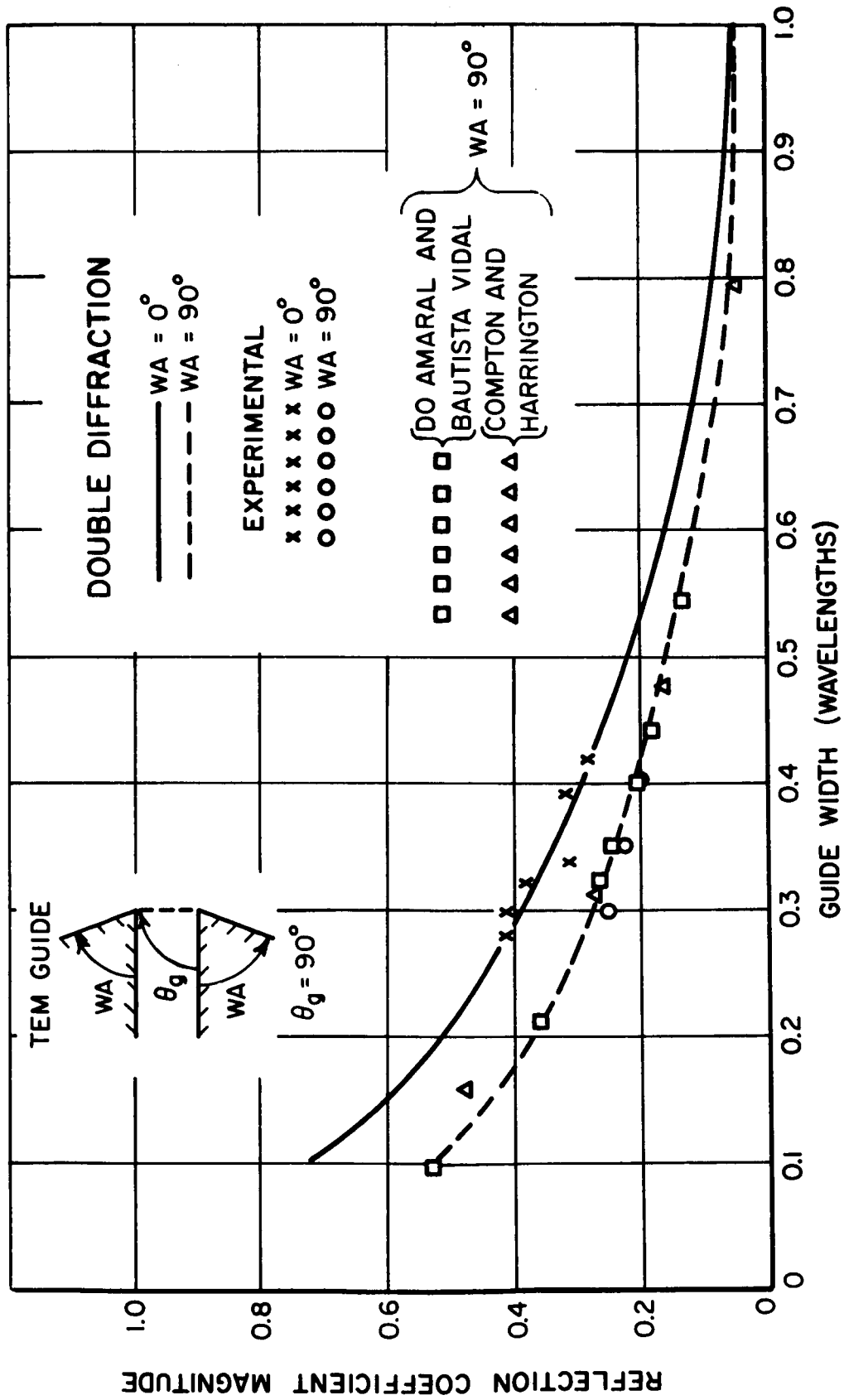


Fig. 16. TEM reflection coefficient magnitude by Double-Diffraction method.

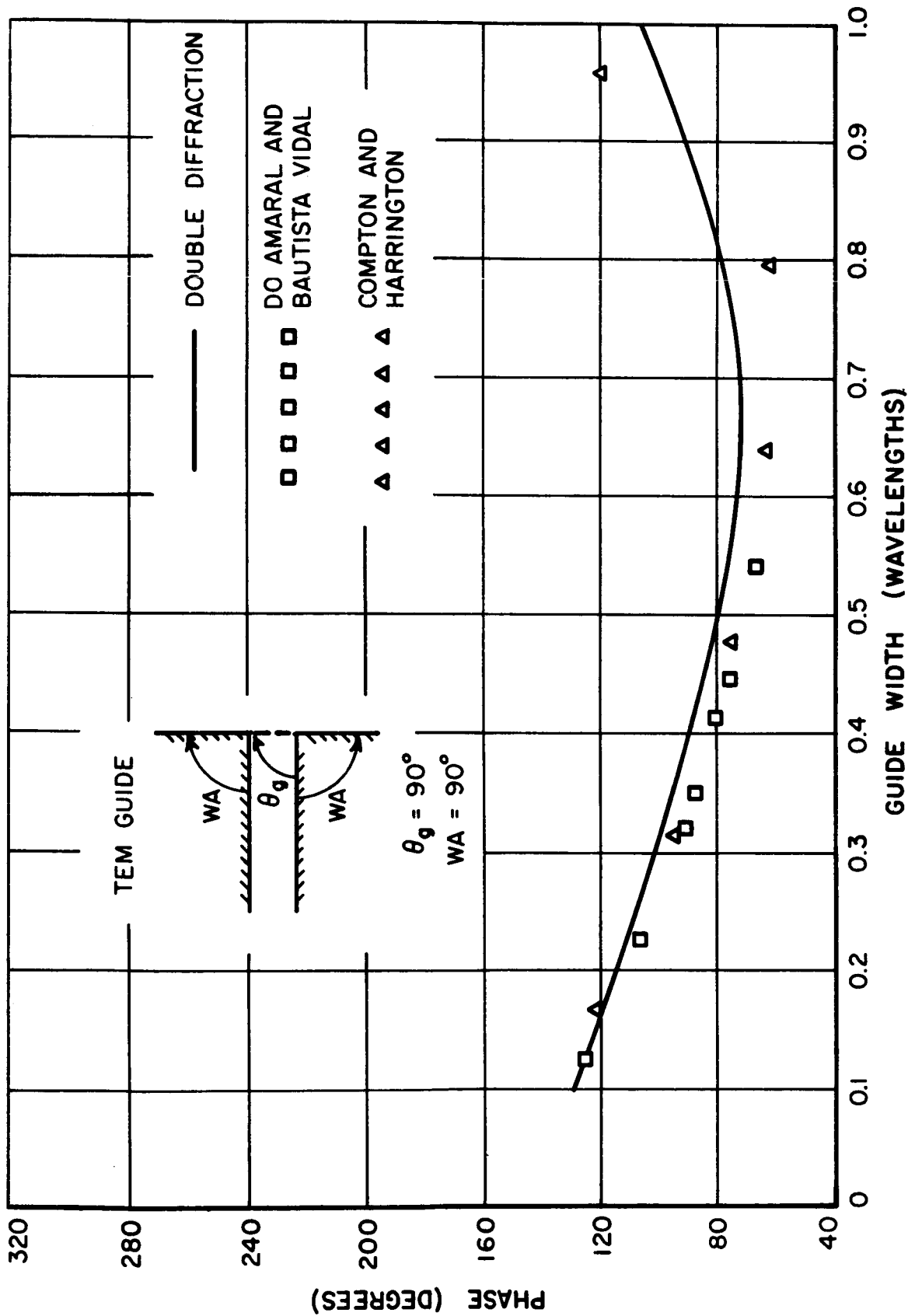


Fig. 17. TEM reflection coefficient phase by Double-Diffraction method.

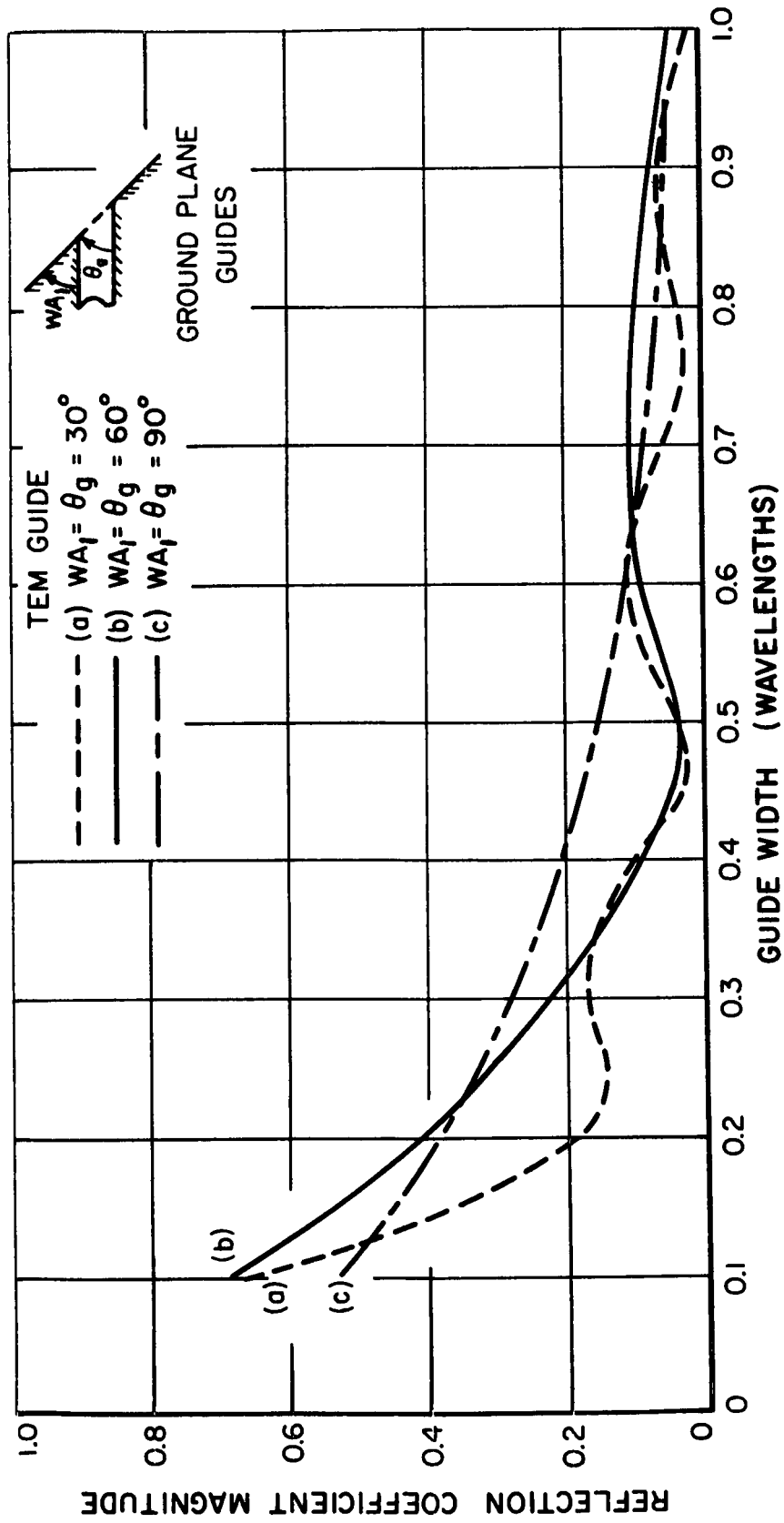


Fig. 18. TEM reflection coefficient magnitude by Double-Diffraction method.

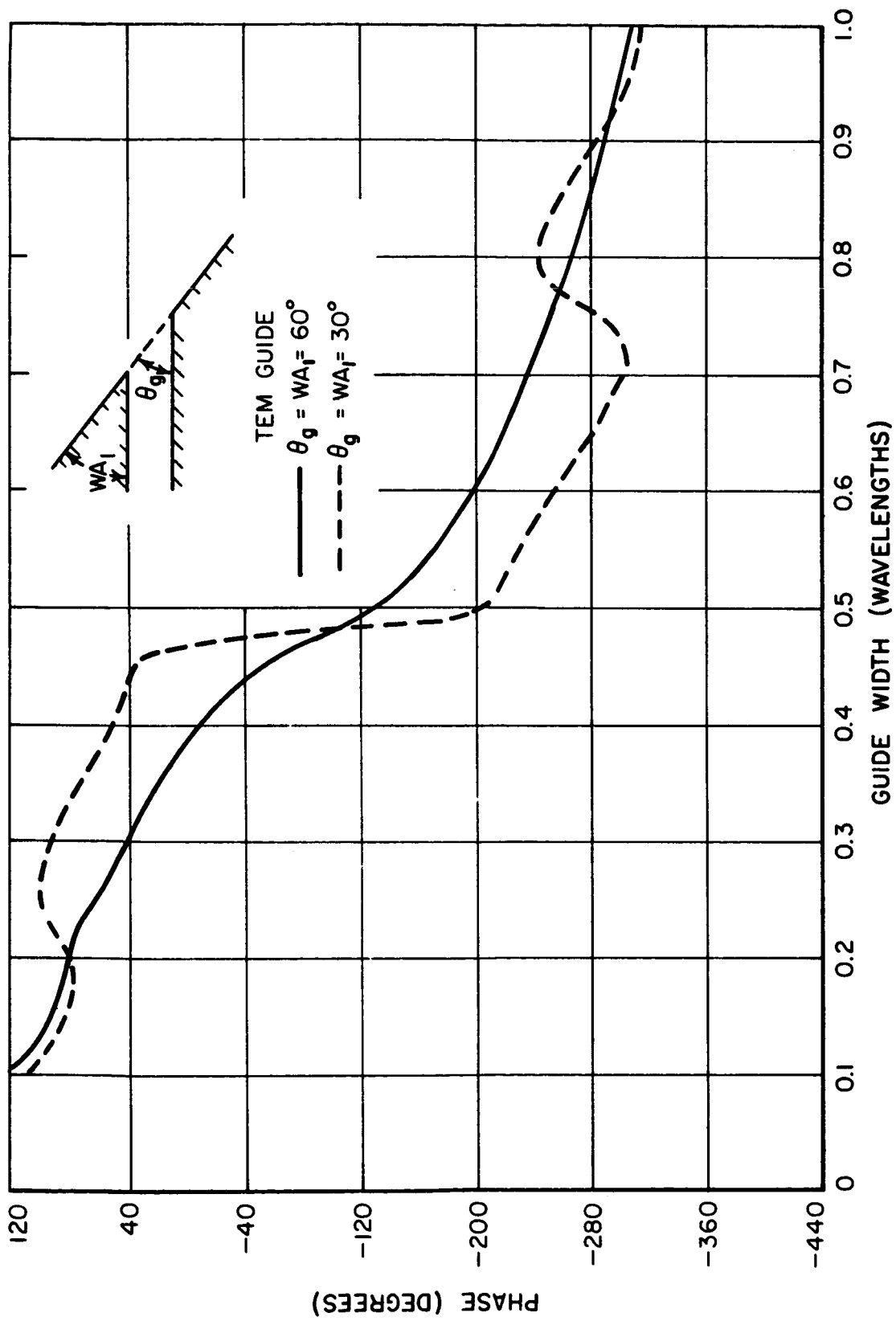


Fig. 19. TEM reflection coefficient phase by Double-Diffraction method.

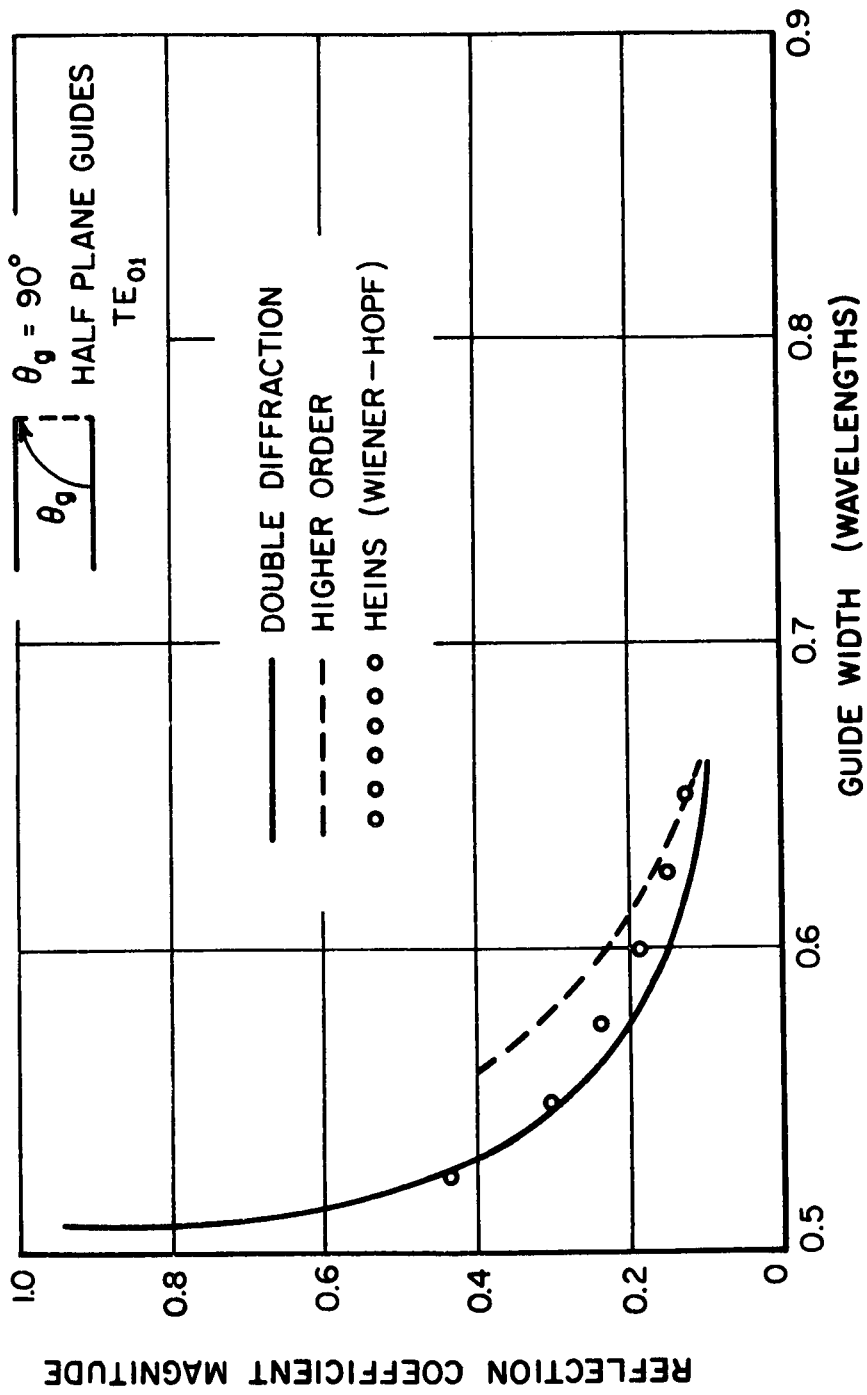


Fig. 20.  $TE_{01}$  reflection coefficient magnitude.

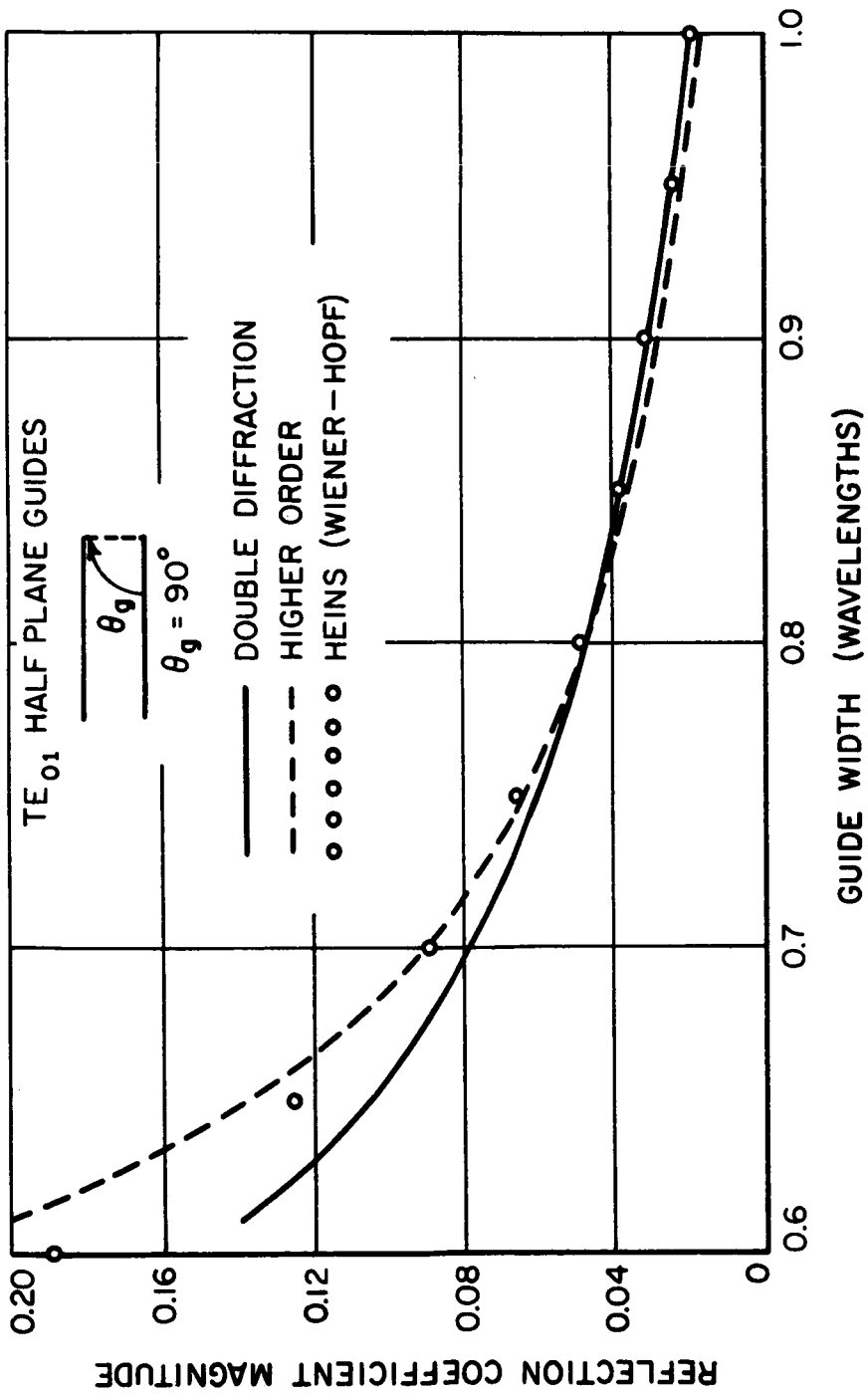


Fig. 21.  $TE_{01}$  reflection coefficient magnitude.

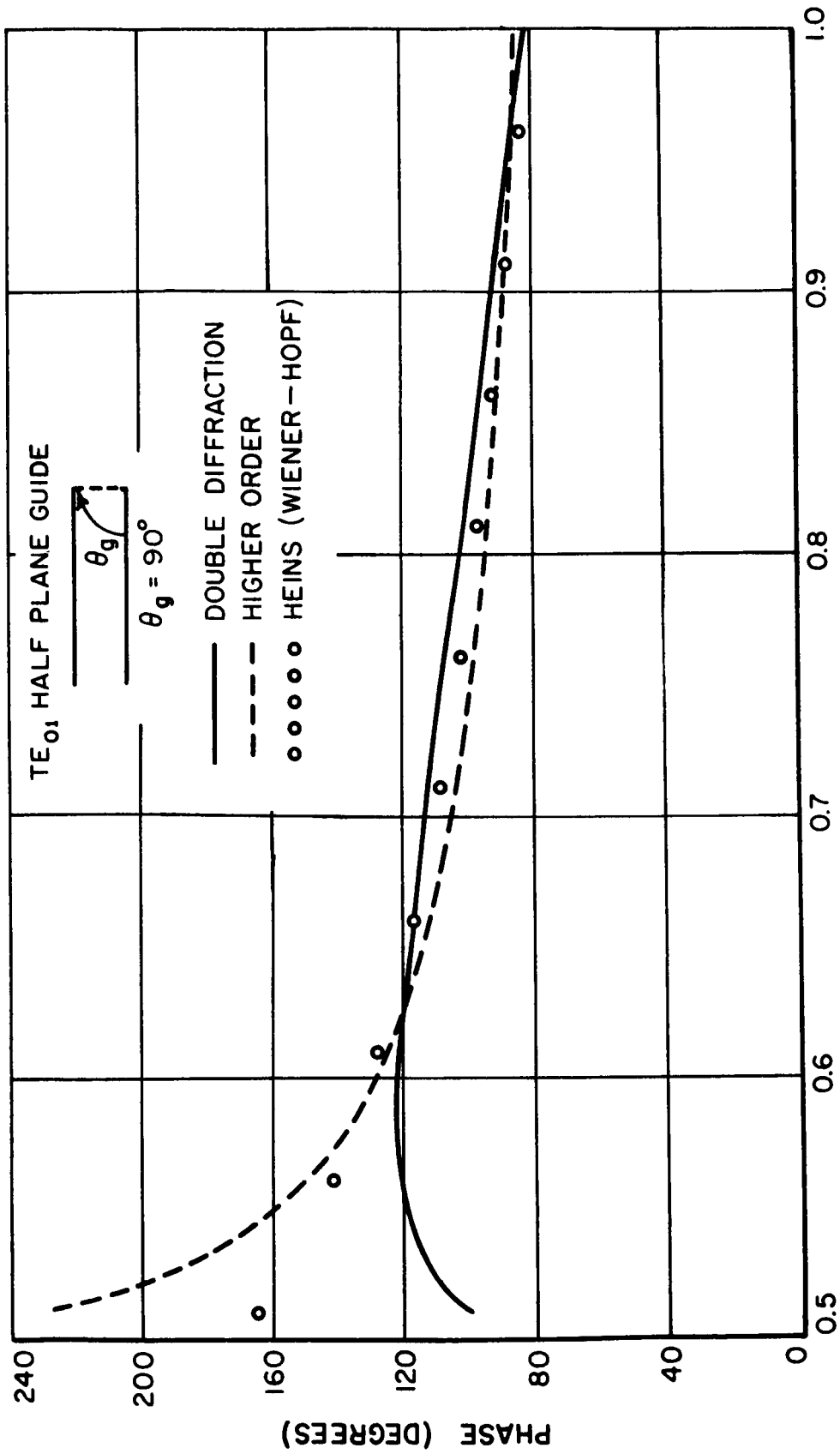


Fig. 22. TE<sub>01</sub> reflection coefficient phase.

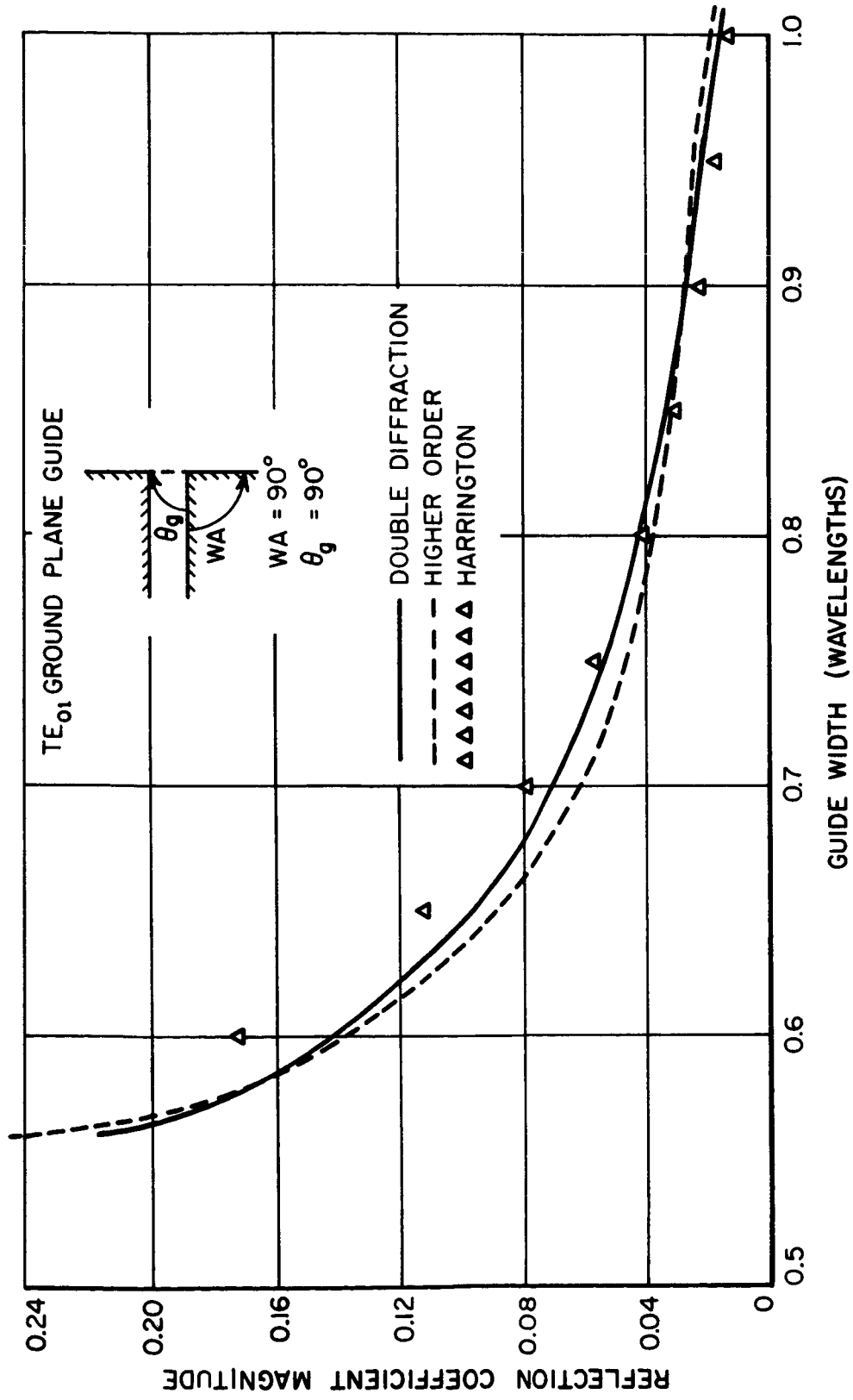


Fig. 23. TE<sub>01</sub> reflection coefficient magnitude.

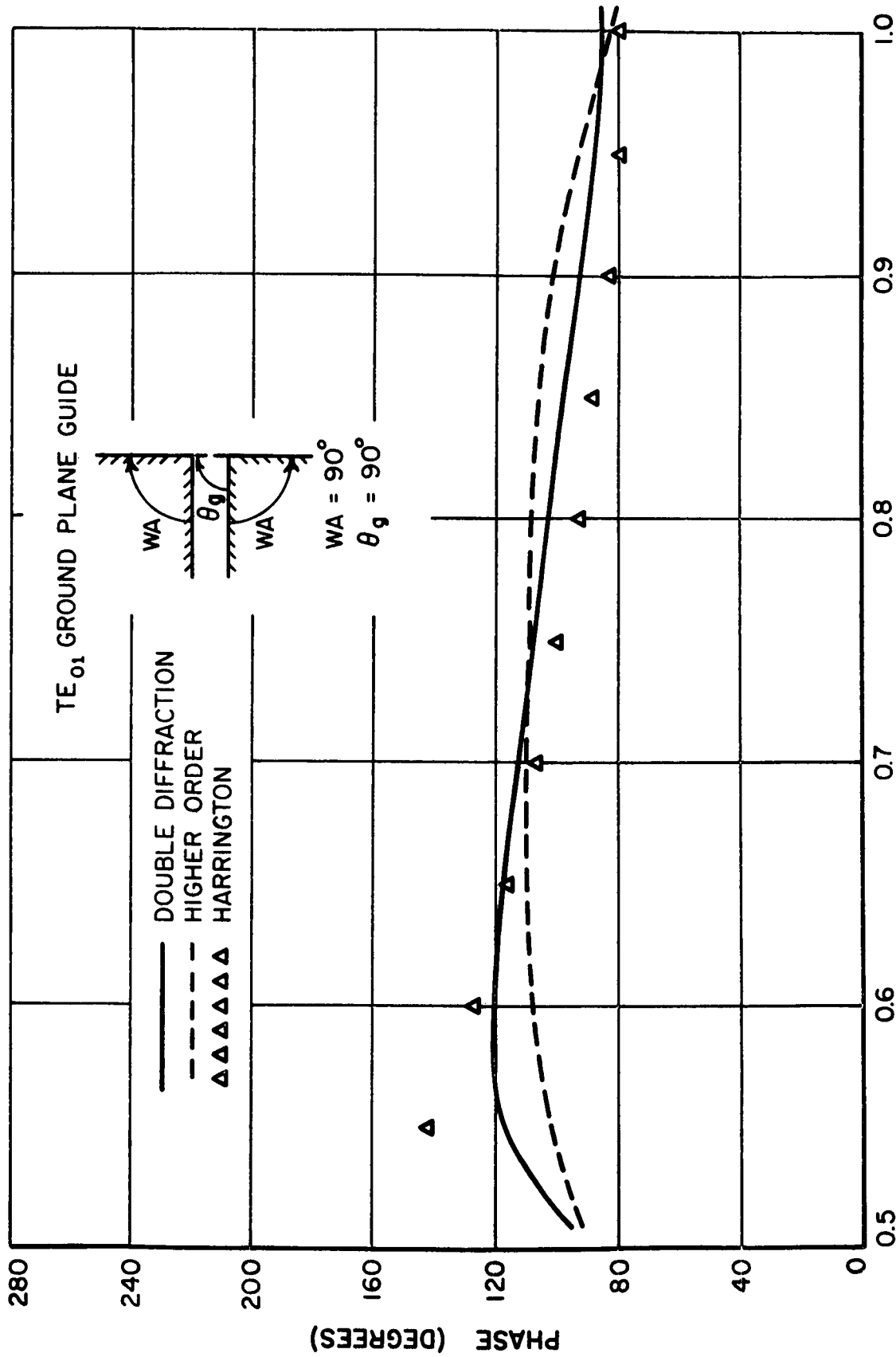


Fig. 24. TE<sub>01</sub> reflection coefficient phase.

## APPENDIX

The reflection coefficient for half-plane ( $WA = 0^\circ$ ), normally truncated ( $\theta_g = 90^\circ$ ), parallel-plate waveguides may be obtained through Wiener-Hopf techniques. For the TEM mode guide, Noble<sup>5</sup> obtained the reflection coefficient as

$$(56) \quad \Gamma = e^{-\frac{1}{2}ka} e^{jka} \left[ \frac{1}{\pi} \left\{ 0.4228 + \ell_n \frac{2\lambda}{a} \right\} \right] \\ \times e^{-j2 \sum_{n=1}^{\infty} \left\{ \sin^{-1} \left( \frac{ka}{2n\pi} \right) - \frac{ka}{2n\pi} \right\}}$$

For the  $TE_{01}$  mode guide Heins<sup>10</sup> obtained the reflection coefficient for  $\lambda/2 < a < \lambda$  as

$$(57) \quad \Gamma = j \left[ \frac{k - \kappa}{k + \kappa} \right]^{\frac{1}{2}} \exp \left[ 2j\theta_1 + 2j \tan^{-1} \left\{ \frac{k - \kappa}{k + \kappa} \right\}^{\frac{1}{2}} + 2\chi(\kappa) \right],$$

where

$$\kappa^2 = k^2 - \left( \frac{\pi}{a} \right)^2,$$

$$\theta_1 = - \sum_{n=1}^{\infty} \left[ \sin^{-1} \left( \frac{\kappa a}{\pi[(2n+1)^2 - 1]^{\frac{1}{2}}} \right) - \frac{\kappa a}{\pi(2n+1)} \right], \text{ and}$$

$$\chi(W) = \frac{jaW}{2\pi} \left[ \ell_n \frac{j\pi}{ak} + 2.4228 \right].$$

## REFERENCES

1. Ryan, C.E., Jr., and Rudduck, R.C., "Calculation of the Radiation Pattern of a General Parallel-Plate Waveguide Aperture for the TEM and TE<sub>01</sub> Waveguide Modes," Report 1693-4, 10 September 1964, Antenna Laboratory, The Ohio State University Research Foundation; prepared under Contract N62269-2184, U.S. Naval Air Development Center, Johnsville, Pennsylvania.
2. Dybdal, R.B.; Rudduck, R.C.; and Tsai, L.L., "Mutual Coupling between TEM and TE<sub>01</sub> Parallel-Plate Waveguide Apertures," IEEE Transactions on Antennas and Propagation, Vol. AP-14, No. 5, (September 1966), pp. 574-580.
3. Rudduck, R.C., "Application of Wedge Diffraction to Antenna Theory," Report 1691-13, 30 June 1965, Antenna Laboratory, The Ohio State University Research Foundation; prepared under Grant NsG-448, National Aeronautics and Space Administration, Office of Grants and Research Contracts, Washington, D.C.
4. Harrington, R.F., Time-Harmonic Electromagnetic Fields, McGraw-Hill Book Company, Inc., New York (1961), pp. 116-120.
5. Noble, B., Methods Based on the Wiener-Hopf Techniques, Pergamon Press, New York (1958), pp. 100-105.
6. Compton, R.T., Jr., "The Admittance of an Infinite Slot Radiating into a Lossy Half-Space," Report 1691-2, 5 October 1963, Antenna Laboratory, The Ohio State University Research Foundation; prepared under Grant NsG-448, National Aeronautics and Space Administration, Office of Grants and Research Contracts, Washington, D.C.
7. Harrington, R.F., op. cit., pp. 180-183.
8. C. Marcio Do Amaral and J.W. Bautista Vidal, "Evanescent-Mode Effects in the Double-Wedge Problem," Appl. Sci. Res., Section B, Vol. 11 (January, 1963), pp. 1-25.

9. Nussenzveig, H.M., "Solution of a Diffraction Problem, I. The Wide Double Wedge, II. The Narrow Double Wedge," Philosophical Transactions of the Royal Society of London, Series A, Mathematical and Physical Sciences, No. 1003, Vol. 252, (15 October 1959), pp. 1-51.
10. Heins, A.E., "The Radiation and Transmission Properties of a Pair of Semi-Infinite Parallel Plates," Quarterly of Applied Mathematics, Vol. 6, (1948-1949), pp. 157-166, 215-220.
11. Harrington, R.F., op. cit., pp. 184-185.

## ACKNOWLEDGEMENT

The authors wish to acknowledge Mr. David C.F. Wu for taking many of the measurements and for his aid in the computations.

9/13/67

*"The aeronautical and space activities of the United States shall be conducted so as to contribute . . . to the expansion of human knowledge of phenomena in the atmosphere and space. The Administration shall provide for the widest practicable and appropriate dissemination of information concerning its activities and the results thereof."*

—NATIONAL AERONAUTICS AND SPACE ACT OF 1958

## NASA SCIENTIFIC AND TECHNICAL PUBLICATIONS

**TECHNICAL REPORTS:** Scientific and technical information considered important, complete, and a lasting contribution to existing knowledge.

**TECHNICAL NOTES:** Information less broad in scope but nevertheless of importance as a contribution to existing knowledge.

**TECHNICAL MEMORANDUMS:** Information receiving limited distribution because of preliminary data, security classification, or other reasons.

**CONTRACTOR REPORTS:** Scientific and technical information generated under a NASA contract or grant and considered an important contribution to existing knowledge.

**TECHNICAL TRANSLATIONS:** Information published in a foreign language considered to merit NASA distribution in English.

**SPECIAL PUBLICATIONS:** Information derived from or of value to NASA activities. Publications include conference proceedings, monographs, data compilations, handbooks, sourcebooks, and special bibliographies.

**TECHNOLOGY UTILIZATION PUBLICATIONS:** Information on technology used by NASA that may be of particular interest in commercial and other non-aerospace applications. Publications include Tech Briefs, Technology Utilization Reports and Notes, and Technology Surveys.

*Details on the availability of these publications may be obtained from:*

SCIENTIFIC AND TECHNICAL INFORMATION DIVISION  
NATIONAL AERONAUTICS AND SPACE ADMINISTRATION

Washington, D.C. 20546